iScience

CellPress
OPEN ACCESS

Article

The effect of the probiotic consortia on SARS-CoV-2 infection in ferrets and on human immune cell response *in vitro*

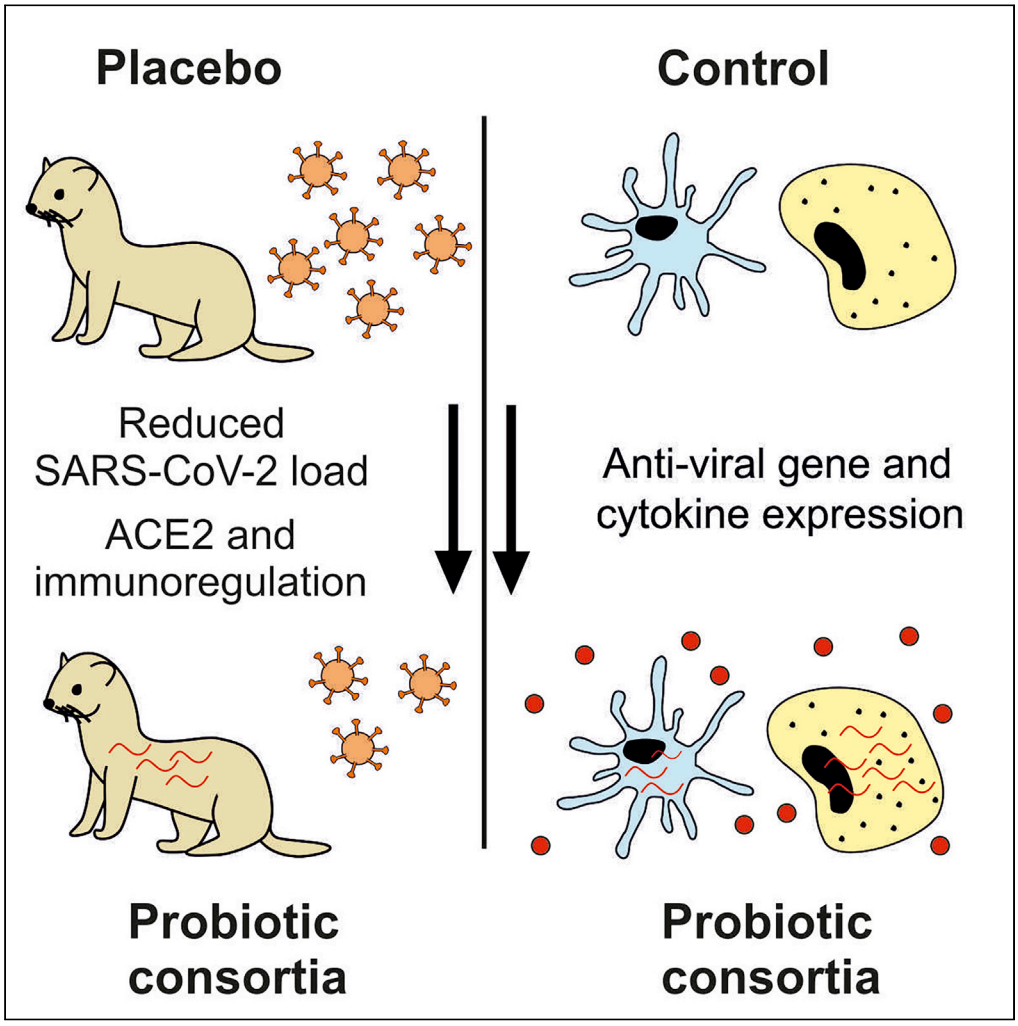

Markus J. Lehtinen, Ritesh Kumar, Bryan Zabel, ..., Sinikka Latvala, Sebastien Guery, Charles R. Budinoff

charles.r.budinoff@iff.com

Highlights

Probiotic consortia decrease SARS-CoV-2 viral load in ferret nasal washes

Ferret duodenal ACE2 but not inflammation was modulated by the consortia

Immune response genes in duodenum and lungs were induced by probiotics

Probiotic consortia induce antiviral response genes in human immune cells *ex vivo*

Lehtinen et al., iScience *25*, 104445
June 17, 2022
https://doi.org/10.1016/j.isci.2022.104445

iScience

CellPress
OPEN ACCESS

Article

The effect of the probiotic consortia on SARS-CoV-2 infection in ferrets and on human immune cell response *in vitro*

Markus J. Lehtinen,[1] Ritesh Kumar,[2] Bryan Zabel,[3] Sanna M. Mäkelä,[1] Derek Nedveck,[3] Peipei Tang,[3] Sinikka Latvala,[1] Sebastien Guery,[4] and Charles R. Budinoff[3,5,*]

SUMMARY

Probiotics have been suggested as one solution to counter detrimental health effects by SARS-CoV-2; however, data so far is scarce. We tested the effect of two probiotic consortia, OL-1 and OL-2, against SARS-CoV-2 in ferrets and assessed their effect on cytokine production and transcriptome in a human monocyte-derived macrophage (Mf) and dendritic cell (DC) model. The results showed that the consortia significantly reduced the viral load, modulated immune response, and regulated viral receptor expression in ferrets compared to placebo. In the human Mf and DC model, OL-1 and OL-2-induced cytokine production and genes related to SARS-CoV-2 antiviral immunity. The study results indicate that probiotic stimulation of the ferret immune system leads to improved antiviral immunity against SARS-COV-2, and the genes and cytokines associated with anti-SARS-CoV-2 immunity are stimulated in human immune cells *in vitro*. The effect of the consortia against SARS-CoV-2 warrants further investigations in human clinical trials.

INTRODUCTION

The emergence and fast spread of severe acute respiratory syndrome coronavirus 2 (SARS-CoV-2) that causes coronavirus disease 2019 (COVID-19) has resulted not only in an acute need for effective therapies and vaccination but also a need for effective dietary strategies for improving immune function. The potential of probiotics — live microorganisms that confer health benefit on the host — in managing SARS-CoV-2 infection has not been extensively studied despite the well-established connection between gut microorganisms and immune function (Hill et al., 2014).

In humans, COVID-19 symptoms vary from mild respiratory symptoms such as fever, fatigue, and dry cough to severe respiratory failure with acute respiratory distress symptoms, acute cardiac injury, and multiorgan failure. Although most individuals subsequently resolve the infection, the disease may also progress to severe pneumonia in susceptible groups. The incubation time of the virus in humans is about 5 days, and severe disease typically develops 8 days after symptom onset, and death occurs at about 16 days (Schultze and Aschenbrenner, 2021).

In February 2020, the World Health Organization (WHO) assembled an international panel to develop animal models for COVID-19 to accelerate the testing of anti-SARS-CoV-2 therapies (Munoz-Fontela et al., 2020). The Ferret model is one of the recommendations by the panel to study SARS-CoV-2. Ferrets (*Mustela putorius furo*) have been used traditionally for testing the pathogenicity and transmission of human respiratory viruses, including influenza. The studies performed so far support the claim that experimental SARS-CoV-2 infection in ferrets results in a predominantly upper respiratory tract infection (Munoz-Fontela et al., 2020). Ferrets are highly susceptible to SARS-CoV-2 and show an increase in viral load, and shed it in nasal washes, saliva, urine, and feces. Ferrets recapitulate the human-to-human transmission but not the severity of the COVID-19 (Kim et al., 2020).

SARS-CoV-2 uses angiotensin-converting enzyme 2 (ACE2) as the main receptor for cell entry (Hoffmann et al., 2020), but with several cofactors involved, including neuropilin-1 (Cantuti-Castelvetri et al., 2020). The domain in ferret ACE2 that binds the spike protein of SARS-CoV-2 differs by two amino acids from its

[1]Health & Biosciences, IFF, Kantvik 02460, Finland

[2]Health & Biosciences, IFF, Wilmington, DE 19803, USA

[3]Health & Biosciences, IFF, Madison, WI 53716, USA

[4]Health & Biosciences, IFF, Niebull 25899, Germany

[5]Lead contact

*Correspondence: charles.r.budinoff@iff.com

https://doi.org/10.1016/j.isci.2022.104445

human homologue and binds to SARS-CoV-2 with similar affinity (Munshi et al., 2021). SARS-CoV-2 primarily infects epithelial cells in the respiratory tract (Alfi et al., 2021), however, infections of the gastrointestinal tract have also been observed (Stanifer et al., 2020) but not extensively studied. In innate immune cells, such as monocytes and macrophages, the infection seems to be abortive (Zheng et al., 2021).

SARS-CoV-2 is an enveloped virus with a +ssRNA genome. The specific innate immune receptors and signaling pathways triggering the interferon (IFN) response in the case of SARS-CoV-2 are yet to be fully determined; however, based on current findings, Toll-like receptor (TLR) 3, TLR7, TLR8, RIG-I, and MDA5 recognize viral RNA and drive MyD88 and NF-κB -dependent pro-inflammatory and type I IFN response that further trigger STAT1, STAT2, and IRF9-dependent induction of IFN-stimulated genes (ISG) (Schultze and Aschenbrenner, 2021). On the other hand, SARS-CoV-2 suppresses the innate immune activation and IFN response to enable its replication in the host cells (Lee et al., 2020; Taefehshokr et al., 2020) that seems to lead to inefficient B cell and T cell responses (Zhou et al., 2020a). Human studies indicate that delayed innate IFN response results at a higher risk to develop severe COVID-19 (Hadjadj et al., 2020). In COVID-19 patients with moderate to severe disease, high chemokine (e.g., CXCL2, CXCL8, CXCL9, and CCL2) and pro-inflammatory cytokine (e.g., interleukin (IL)-1β, IL-6, and IL-1Ra) response was detected in bronchoalveolar lavage fluid (BALF) (Zhou et al., 2020b) in postmortem lung biopsies and serum samples (Blanco-Melo et al., 2020) but without significant upregulation of type I or type III IFNs, although ISGs from e.g., IFIT and IFITM families were induced. Accordingly, intranasal IFN-I administered pre-virus or post-virus challenge reduced disease burden (Hoagland et al., 2021). The aforementioned studies suggest that stimulation of innate immune function could be beneficial in controlling the viral replication and eradication.

In the past two decades, the effects of probiotics on immune function and respiratory viral infections have been studied in numerous clinical studies but with variable quality. Although meta-analyses indicate efficacy of probiotics against acute upper respiratory tract (URT) infections in general (Hao et al., 2015; King et al., 2014; Shi et al., 2021), the results per strain vary, and accordingly, probiotic effects on immunity should be investigated on a per strain or consortia basis (Hill et al., 2014). Clinical studies on specific strains like *Bifidobacterium (B.) lactis* BI-04 showed that specific probiotics can reduce the risk of URT illness episodes in healthy adults (West et al., 2014) or reduce rhinovirus load in human nasal wash samples (Turner et al., 2017). The clinical and preclinical evidence suggest that use of probiotics could prime the immune system before viral infection (Lehtoranta et al., 2020). For example, *Lactobacillus (L.) acidophilus* NCFM induced the upregulation of TLR3, IL-12, and IFN-β in murine DCs (Weiss et al., 2010) and *Lacticaseibacillus* strains inhibited influenza A replication in human monocyte-derived macrophages (Miettinen et al., 2012).

One of the hypotheses for the probiotic mode of actions against SARS-CoV-2 respiratory and intestinal infection is via strengthening the gut epithelial barrier and beneficial modulation of the gut microbiota and the immune system (Harper et al., 2021). Age and comorbidities that make people more susceptible to severe COVID-19 are associated with perturbed gut microbiota, dysbiosis, and decrease in epithelial barrier integrity in the gut (Vignesh et al., 2021). SARS-CoV-2 infects gut epithelial cells (Stanifer et al., 2020), which may cause lipopolysaccharide (LPS) and other pathogen-associated molecular patterns (PAMPs) to leak across the epithelial barrier. The resulting innate immune activation via the gut-lung-axis may contribute to the cytokine storm in these individuals (Vignesh et al., 2021).

To investigate the effect and mechanism of action of probiotics against SARS-CoV-2, we designed two probiotic consortia to stimulate innate immune function against SARS-CoV-2: OL-1 (*B. lactis* BI-04, *B. longum* subsp. *infantis* Bi-26, *Lacticaseibacillus rhamnosus* Lr-32, *Lacticaseibacillus paracasei* Lpc-37, *Ligilactobacillus salivarius* Ls-33) and OL-2 (*B. lactis* Bi-07, *L. acidophilus* NCFM, *Limosilactibacillus fermentum* SBS-1, *Lactococcus lactis* LI-23, *Streptococcus thermophilus* St-21). We tested the effect of the probiotic consortia in a ferret SARS-CoV-2 challenge model and in human monocyte-derived macrophage (Mf) and dendritic cell (DC) model. The results in ferrets show that OL-1 and OL-2 modulate the duodenal and lung immune response during infection, ACE2 expression in duodenum, and reduce SARS-CoV-2 viral load in nasal washes. We further show that the exposure of OL-1 and OL-2 to human monocyte-derived Mfs and DCs results in upregulation of genes and cytokines critical for early innate immune activation against SARS-CoV-2.

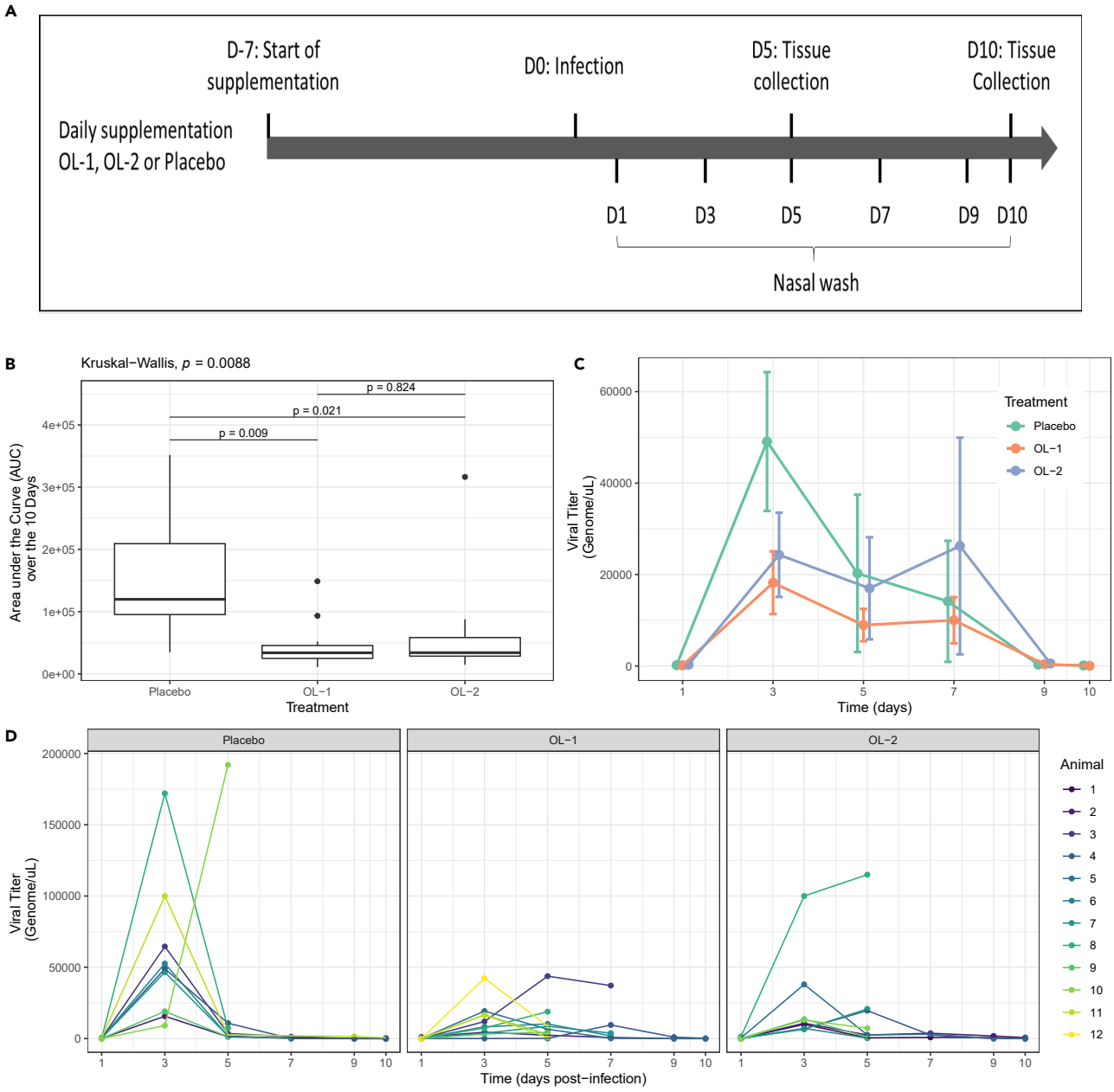

Figure 1. The main ferret study and nasal wash viral load analysis

The ferrets were supplemented with OL-1 or OL-2 or placebo and infected with SARS-CoV-2.

(A–D) (A) The ferret study design and time points for treatment supplementation, SARS-CoV-2 infection, tissue and nasal wash collection (D = Day); (B) The nasal wash viral load AUC analysis (Line: median Box: lower and upper quartile, Whiskers: min and max; Kruskal-Wallis test and pairwise Wilcoxon tests) (C) The nasal wash viral load time point analysis (Symbol: mean; error bars: standard error: note that at day 1 all groups have nonzero values (means of 152, 297, and 201 genome/μL for OL-1, OL-2, and placebo, respectively); (D) Time course of individual viral loads in nasal washes from ferrets.

RESULTS

Probiotic consortia decrease the nasal wash SARS-CoV-2 titers in ferrets

Ferrets have been shown to model SARS-CoV-2 replication and infection in the airways and to express ACE2 (Kim et al., 2020). We evaluated the effect of the two probiotic consortia OL-1 and OL-2 on the SARS-CoV-2 infection, ACE2 expression, and immune function in ferrets in two placebo-controlled studies: main (Figure 1) and pilot (Figure S1). The pilot study was run early after the onset of the COVID-19 pandemic

to better understand the model, whereas the main study included changes to the protocol based on the learnings from the pilot study and was aimed to test the efficacy of the OL-1 and OL-2.

In the main study, probiotic consortia were supplemented 7 days (D) before (D-7) viral infection (D0) and until D10 postinfection. Lung and duodenum samples were gathered for qPCR gene expression analysis (D5 and D10) and tissue staining (D5 and D10), and nasal washes were collected D1-D10 for determining the viral load by qPCR (Figure 1A). The SARS-CoV-2 viral load over the infection time (D1-D10) showed statistically significant differences in the area under the curve (AUC) between the OL-1, OL-2, and placebo groups ($p = 0.0088$; Kruskall-Wallis). Note that at day 1, all groups have nonzero values (means of 152, 297, and 201 genome/μL for OL-1, OL-2, and placebo, respectively) (Figure 1B). *Post hoc* pairwise Wilcoxon tests further demonstrated the significant differences in AUC between the placebo and the OL-1 ($p = 0.009$) and OL-2 ($p = 0.021$) groups, respectively. On average, OL-1 and OL-2 reduced the AUC by 68 and 52%, respectively, as compared to the placebo group, suggesting influence of the probiotic consortia on the antiviral immunity against SARS-CoV-2.

The time-course analysis of the SARS-CoV-2 nasal wash qPCR showed that the viral loads peaked in general at D3 (average viral titer of 4.9×10^4 genome/μL, 1.8×10^4 genome/μL, and 2.4×10^4 genome/μL in the Placebo, OL-1, and OL-2 groups, respectively) and were mostly resolved by D9 (average viral titer of 319 genome/μL, 394 genome/μL, and 552 genome/μL in the placebo, OL-1, and OL-2 groups, respectively) (Figure 1C). In addition, investigation of the individual line plots (Figure 1D) showed that the viral loads of few animals show later peaking (1/9, 5/11, and 3/9 animals in the placebo, OL-1, and OL-2 groups, respectively). Most-later peaking animals were found in the treatment groups that could reflect the effects observed on the viral replication.

In comparison to the main study, the pilot study had a different probiotic supplementation regime, where OL-1 was administered 21 days before infection (D-21) and OL-2 one day postinfection (D1) (Figure S1). The viral load analysis showed undetectable to very low viral genomes in the samples (Figure S1) despite the use of the same viral dose to induce the infection and housing dependent infectivity. The pilot study did not show a treatment effect on the viral load. To further understand why the viral load was low or absent in the pilot study or any treatment effects, the lung and duodenum samples at D0 (preinfection), D5, and D21 were collected for later qPCR analyses; in addition, D0 samples were used later as a comparator for the main study responses.

The body temperature of the ferrets and visual symptoms of viral infection were monitored in both studies. The SARS-CoV-2 infection in ferrets did not affect the body temperature, body weight, or induce coughing, sneezing, or dyspnea in the animals during infection, in line with previous literature (Peacock et al., 2021; Ryan et al., 2021).

Lung and duodenal gene expression show changes by probiotic consortia

To understand further the differences in immune response between the pilot and the main study, ferret immune response to SARS-CoV-2, and the mechanism of action of OL-1 and OL-2 on the lung viral load decrease, lung and duodenal tissues from the main (Figure 1A) and the pilot study (Figure S1) were collected, and gene expression was measured using qPCR (Figures S2 and 2).

First, we wanted to understand the effect of the virus infection on the immune response. Importantly, preinfection samples (D0) were taken only for the OL-1 and placebo groups from the pilot study. Ferrets in the study were outbred, had the placebo from the same batch, and the virus was known to cause a strong immune response that is clearly different from the potential small differences in the baseline immunity between the main and the pilot study; therefore, we decided to use D0 noninfected placebo group samples from the pilot study as a baseline to normalize not only the pilot (Figure S2A) but also the main study (Figure S2B) immune response data to the SARS-CoV-2 infection. Statistical analysis indicated only minor changes in the pilot study for lung and duodenal gene expression (Figure S2A), in line with the low infectivity in the experiment. Instead, in the main study, IFN (*IFNA* and *IFNL1*), cytokine (*IL-10*), and chemokine (*CCL2, IL8*) gene expression was increased in responses to the SARS-CoV-2 infection in all the treatment groups (adjusted $p < 0.1$; FDR) (Figure S2B). It is noteworthy that *IFNG* expression was downregulated in the lung tissue and *ACE2* expression was downregulated in the duodenum, whereas it was upregulated in the lungs (Figure S2B). At D5 both consortia, but not placebo, had a significant increase in *CXCL10* in

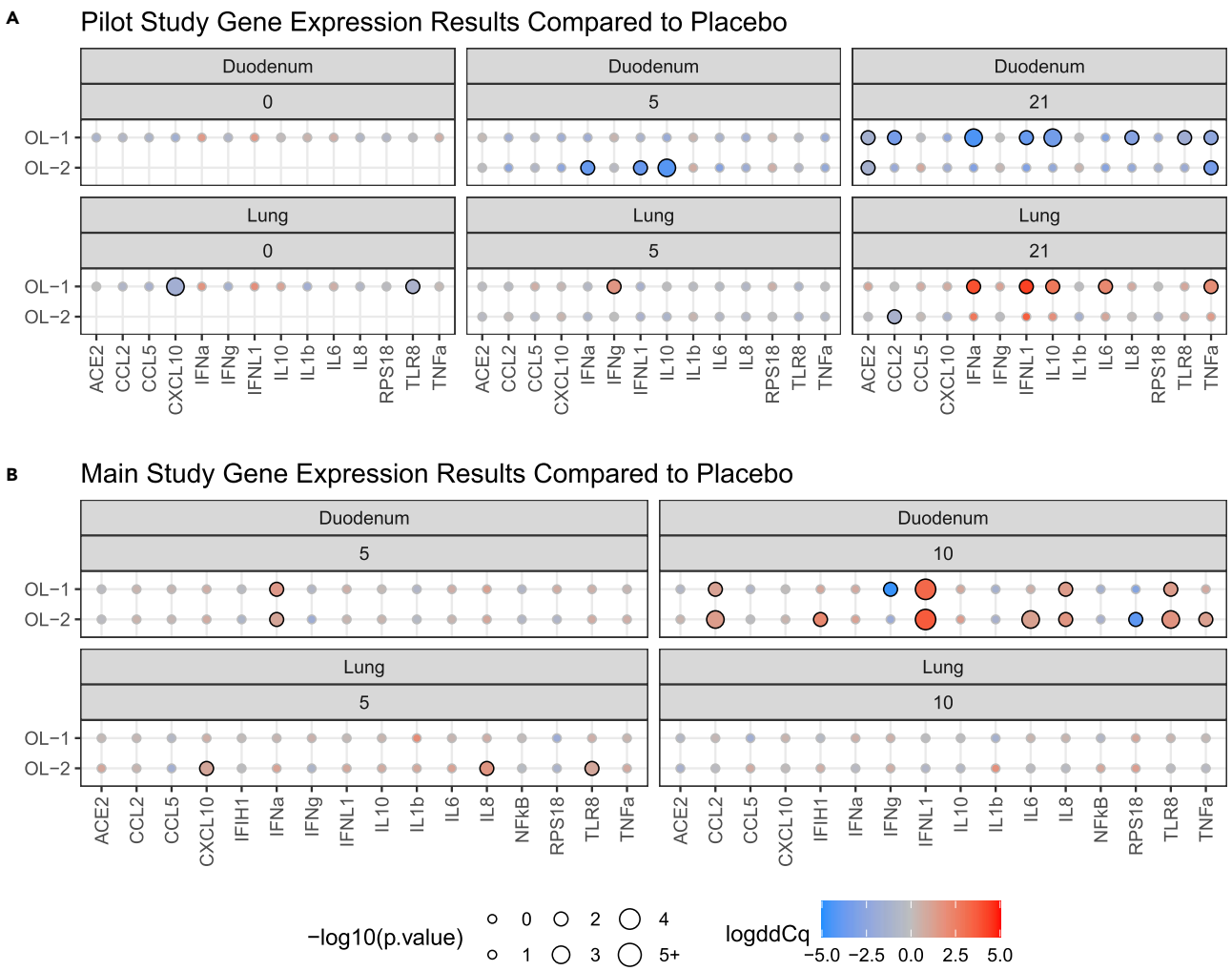

Figure 2. The effect of the treatments on the immune marker gene expression of the ferrets infected with SARS-CoV-2

Balloon plots showing gene expression levels as log2 fold changes for the pilot and main studies. Placebo treatments at the same time points for (A) the pilot and (B) the main study was used as the comparator. Color of balloons denotes direction and magnitude of log2 fold change, with blue showing a decreased log2 fold change relative to the placebo, and red and increased log2 fold change. Size of the balloons corresponds to the –log10 of the p value (adjusted with the Tukey method for a family of estimates) from a post hoc pairwise comparison of the estimated marginal means to the placebo reference; larger balloons mean a smaller p value. Statistically significant fold changes are marked by a black outline around the balloon (p value < 0.1).

duodenum and lungs (adjusted $p < 0.1$; FDR) (Figure S2B). As there was not a noninfected placebo group in the main study, the results (Figure S2B) should be interpreted cautiously. In summary and based on the viral load and qPCR results the main study seems to model better SARS-CoV-2 infection and immune response, whereas in the pilot study the infectivity and immune response is less apparent.

To compare the effect of OL-1 and OL-2 to placebo, we did a within study time point comparison of the qPCR data for the pilot (Figure 2A) and the main study (Figure 2B). In the main study, expression of several immune genes was regulated by OL-1 and OL-2 in time point comparison to the placebo group (Figure 2B). At D5 both consortia induced upregulation of *IFNA* in the duodenum, and OL-1 further upregulated *CXCL10*, *IL8*, and *TLR8* in the lungs compared to placebo (adjusted $p < 0.1$; FDR). At D10 both consortia had higher *CCL2*, *IFNL1*, *IL8*, and *TLR8* gene expression in duodenum compared to placebo (adjusted $p < 0.1$; FDR). In addition, OL-1 had a decrease in *IFNG* expression; on the other hand, OL-2 increased *IFIH1*, *IL6*, and *TNFA* (adjusted $p < 0.1$; FDR) (Figure 2B). In the lungs, there were no significant differences at D10 between the groups. Overall, the results indicate stronger immunomodulation in the duodenum and also effects in the lungs, in line with the route of administration by gavage.

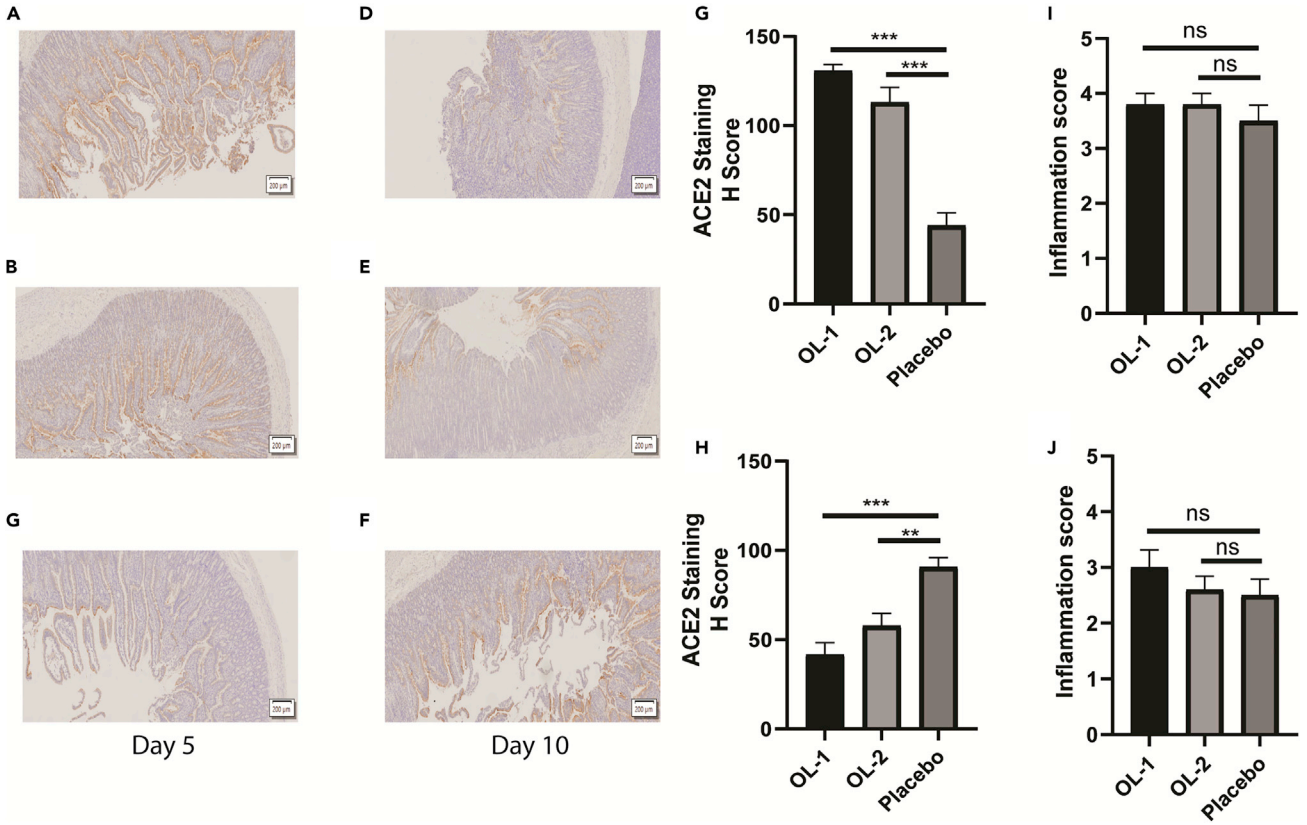

Figure 3. Localization and expression of ACE2 and inflammatory scoring in duodenum

Representative images and quantification of ACE2 immunohistochemical staining from the main study. Panels (A–C) are from D5 and (D)–(F) are from D10. (A) and (D) are from OL-1, (B) and (E) are from OL-2 and (C) and (F) are from placebo groups. (G) Quantification of ACE2 expression for D5. (H) Quantification of ACE2 expression for D10. (I) and (J) H&E-stained duodenum sections were evaluated for inflammation (0 no inflammation to 4 severe inflammation) and average inflammation score for each treatment group is shown in (I) for D5 and (J) for D10. Data is presented as mean ± SEM. Statistical analysis was performed using one-way ANOVA followed by Dunnett's multiple comparisons test. ns, not significant, **, $p < 0.01$; ***, $p < 0.001$.

In the pilot study, there were minor differences at D0 and D5. At preinfection (D0), OL-1 decreased *CXCL10* and *TLR8* expression in the lung samples (adjusted $p < 0.1$; FDR) (Figure 2A), indicating potential influence of the supplementation alone on the lungs. At D5 OL-2 decreased *IFNA*, *IFNL1*, and *IL10* in duodenum, and OL-1 increased *IFNG* expression in lungs (adjusted $p < 0.1$; FDR) (Figure 2A), suggesting influence on the IFN responses. At D21, when the infection was cleared, OL-1 had broadly decreased expression of cytokines and IFNs in the duodenum and an increase in *IFNA, IFNL1, IL10, IL6,* and *TNFA* in lungs (adjusted $p < 0.1$; FDR). In addition, both consortia decreased ACE2 expression in the duodenum (adjusted $p < 0.1$; FDR) (Figure 2A). The results at D21 could be an indication of postinfection influence of the probiotic consortia on the recovery from the infection.

It should be noted that the postinfection gene-expression results regarding the OL-1 and OL-2 effect compared to placebo were different between the pilot (D5 and D21) (Figure 2A) and the main study (D5 and D10) (Figure 2B). We think that the main factor driving the difference was the lower level of infection in the pilot study that resulted in significantly different profile and lower level of SARS-CoV-2-induced gene expression than in the main study (Figure S2). Thus, the anti-SARS-CoV-2 immune responses that the probiotic consortia are modulating are different, as are then the probiotic consortia effects compared to placebo, on that immune response in the pilot (Figure 2A) and in the main study (Figure 2B). In conclusion, the probiotic effects between the pilot and the main study are not directly comparable.

Probiotic consortia modulate duodenal ACE2 surface expression

In the qPCR analysis of the pilot study, we found a decrease of *ACE2* expression at D21 in duodenum (Figure 2C). As humans have gastrointestinal symptoms and potential viral replication in the gut, we wanted to

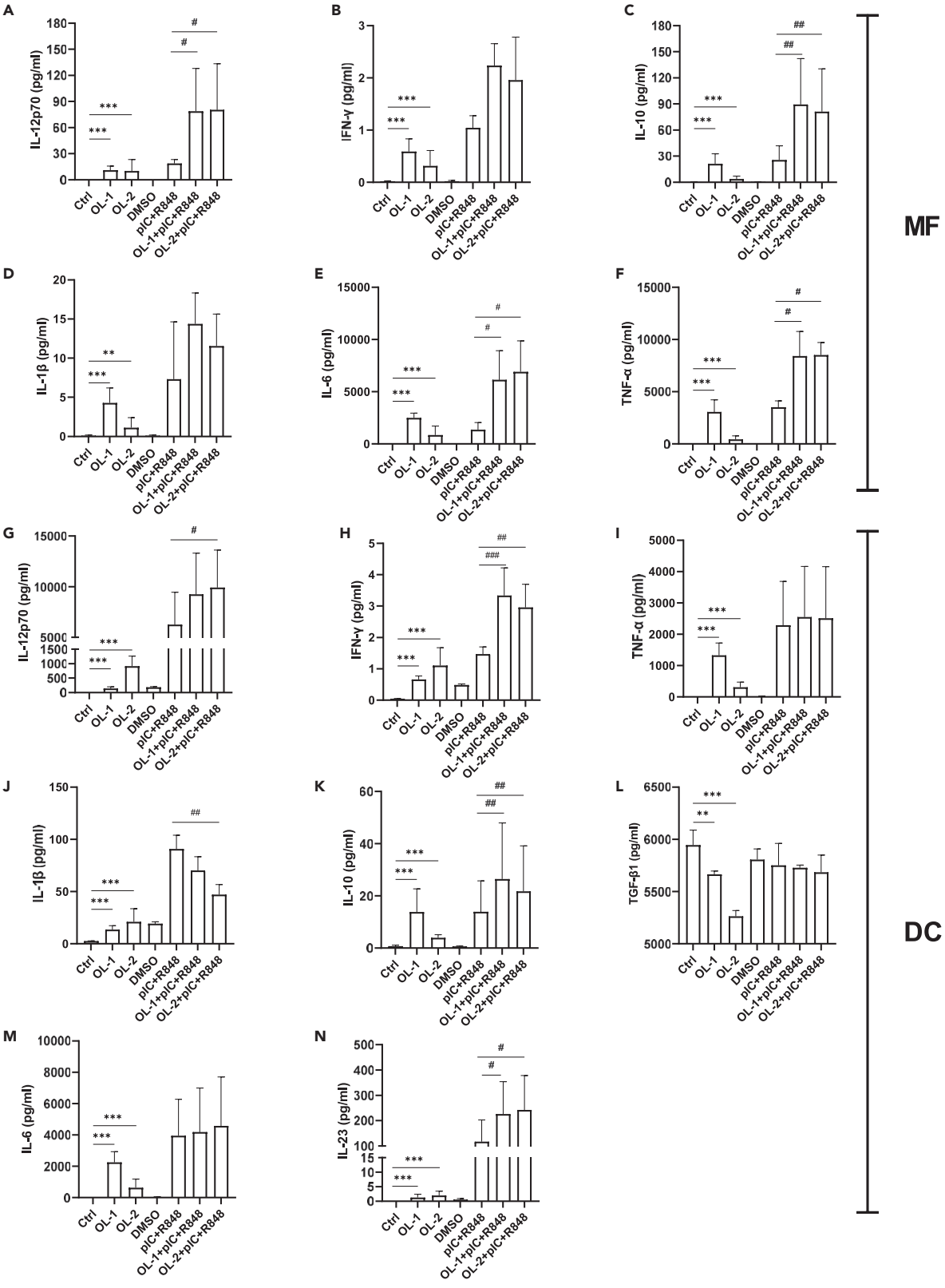
A
IL-12p70 (pg/ml)
B
IFN-γ (pg/ml)
C
IL-10 (pg/ml)
D
IL-1β (pg/ml)
E
IL-6 (pg/ml)
F
TNF-α (pg/ml)
MF
G
IL-12p70 (pg/ml)
H
IFN-γ (pg/ml)
I
TNF-α (pg/ml)
J
IL-1β (pg/ml)
K
IL-10 (pg/ml)
L
TGF-β1 (pg/ml)
M
IL-6 (pg/ml)
N
IL-23 (pg/ml)
DC
Ctrl
OL-1
OL-2
DMSO
pIC+R848
OL-1+pIC+R848
OL-2+pIC+R848

Figure 4. The effect of the consortia and pIC+R848 on human macrophage and dendritic cell cytokine response

Mfs and DCs were incubated with the treatments, for 24 and 48 h, respectively. Cytokine concentrations in the supernatants were measured with ELISA and the mean of four donors (pg/mL) with standard deviation is shown. DMSO, dimethyl sulfoxide was used as a vehicle control for pIC+R848. The data was analyzed with a linear model using change from a baseline as response (Ctrl vs OL-1 or OL-2; or pIC+R848 vs OL-1+pIC+R848 or OL-2+pIC+R848). N = 4, *p = 0.01 =< 0.05; **p = 0.001 =< 0.01; ***p < 0.001 vs ctrl and #p = 0.01 =< 0.05; ##p = 0.001 =< 0.01; ###p < 0.001 vs pIC+R848.

further determine by tissue staining if the probiotic supplementation would influence viral receptor ACE2 expression and inflammation in the duodenal tissues (Figure 3). For ACE2, during acute infection at D5, OL-1 and OL-2 group tissue sections had increased staining compared to placebo group ($p < 0.01$; ANOVA, Dunnett's) (Figures 3A–3C and 3G), suggesting cytoprotective effects during inflammation. At D10, during the resolution phase of the infection, the ACE2 staining was decreased in OL-1 and OL-2 groups compared to D5 and to placebo ($p < 0.01$; ANOVA, Dunnett's) (Figures 3D–3F and 3H). The results suggest differential effects of the OL-1 and OL-2 compared to placebo on ACE2 cell surface expression over the course of infection. These observations suggest that ACE2 expression is very dynamic and may depend upon viral load and level of infection. It is noteworthy that as we did not have the preinfection D0 staining samples for ACE2, the normal level of ACE2 is not known.

The inflammatory scorings of the tissue sections showed severe inflammation in all the treatment groups and gradual resolution by D10 (Average score of 3.5 at D5, and 2.5 at D10 of maximum 4.0 in all groups), supporting the result of the increase in inflammatory gene expression levels by qPCR (Figure S2B). However, the fecal pellets remained of normal consistency in the ferrets. The treatments with OL-1 or OL-2 did not have an effect on the duodenal inflammation scores ($p > 0.05$; ANOVA, Dunnett's).

Human macrophages and dendritic cells are stimulated by OL-1 and OL-2

To test how OL-1 and OL-2 could potentially influence anti-SARS-CoV-2 immunity in humans, we used fresh human peripheral blood monocyte-derived macrophages (Mf) and dendritic cells (DC). The immune cells from four donors without technical replicates were incubated with OL-1, OL-2, controls, or TLR agonist mix Poly I:C (pIC) (TLR3) and R848 (TLR7/8) – that mimics immune response to viral RNA. We also used the combination of pIC + R848 with OL-1 or OL-2 to evaluate modulation of the cell response to pIC + R848 by the consortia (Figure 4).

Incubation of the OL-1 or OL-2 with Mfs for 24 h resulted in an increase in all the measured cytokines from supernatant by ELISA of which IL-6 and TNF-α had most pronounced increase, followed by IL-10, IL-12p70, IFN-γ, and IL-1β (Figures 4A–4F). Increase in cytokine production and type I immunity cytokines indicate Mf activation by both consortia. Modulation of pIC+R848 response by OL-1 and OL-2 resulted in an enhanced response to IL-6, IL-10, IL-12p70, and TNF-α (Figures 4A–4F), indicating additive stimulation of both pro-inflammatory and anti-inflammatory responses during TLR3 and TLR7/8 stimulation.

After 48 h of incubation with DCs both consortia increased secretion of IL-12p70 compared to control (Figure 4G) and IFN-γ with or without pIC+R848 (Figure 4H), indicating Th1 polarization of the DCs by both consortia directly but also augmentation of Th1 response upon TLR3 and TLR7/8 stimulation. TNF-α and IL-1β may support Th1 polarization of DCs; however, the effects of the consortia on the cytokine production were mixed as direct incubation increased TNF-α and IL-1β; but in the pIC+R848 response modulation, there was either no effect or decrease of IL-1β in OL-2 samples (Figures 4I and 4J). Both consortia increased IL-10 production (Figure 4K) but suppressed TGF-β (Figure 4L), supporting polarization toward Th1, although some potentiation of the Th17 polarizing cytokines IL-23 and IL-6 secretion was observed (Figures 4M and 4N). In summary, the results suggest that consortia could drive polarization of the DCs towards Th1 cell induction but with some induction of Treg and Th17-associated cytokines.

Probiotic consortia induce innate immune transcriptomes in macrophages and dendritic cells

To further test the effect of OL-1 and OL-2 on immune cell stimulation and to compare to pIC+R848 response, we conducted transcriptomic analyses. Briefly, RNA was extracted for sequencing from all treated groups of Mfs and DCs from the experiments described before and at the same time points than ELISA samples were taken (Figure 4).

To gain an initial broad view of the transcriptome profiles, we conducted a principal component analysis (PCA). In the analysis of the full dataset, *i.e.*, DC and Mf samples together, PC1 captured 70% and PC2

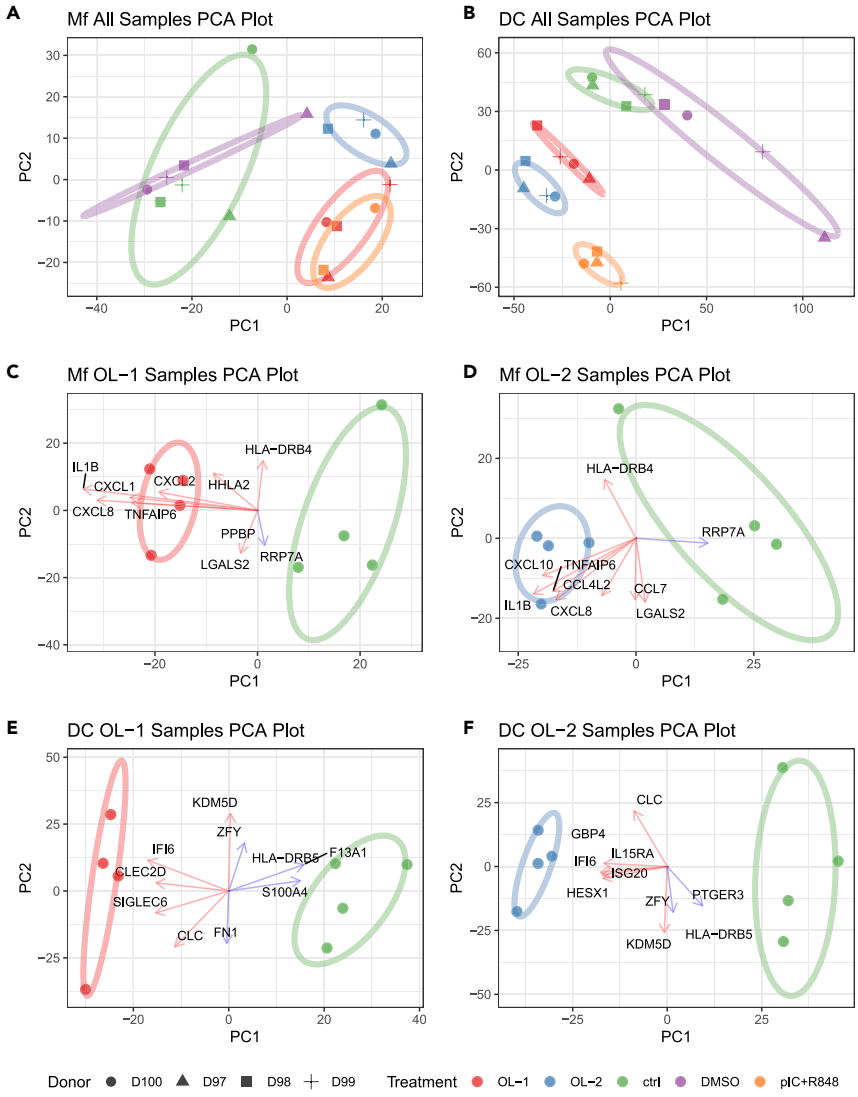

Figure 5. Global transcriptomics analyses of OL-1, OL-2, and pIC+R848 stimulated macrophages and dendritic cells

(A–F) Principal component analysis (PCA) of transcriptomes of all samples tested for Mf (A) and DC (B). PCA plots including top gene loadings for Mf samples compared to the control for OL-1 (C) and OL-2 (E) and for Mf cells OL-1 (D) and DC (F). Color of the individual points and collective ellipses denotes treatment. Each point is an individual sample transcriptome containing all genes expressed. Shapes in panels A and B indicate the blood donor used. PC loadings are shown for OL-1 and OL-2 alone samples as arrows showing the effect of specific genes on the variation of the PCA plot. Arrows denote directionality of the variation and the value represents a graphical representation of the variation (in scale relation to each other but not number on the scale) in either PC1 (horizontal axis) or PC2 (vertical). Color of the arrows represents the gene being upregulated (red) or downregulated (blue) in OL-1 or OL-2 vs ctrl comparison.

14% of the variance, accounting for the differences in the cell type and the treatment effect, respectively. As the cell type was the largest driver of variation, further PCA was conducted by the cell type (Mfs and DCs were analyzed separately). In the Mf and DC specific PCAs, the donor samples clustered together based on treatment and did not show any extreme outliers (Figures 5A and 5B).

The PCA of the Mf data resulted in the separation of OL-1, OL-2, and pIC+R848 from the controls (DMSO and ctrl, PC1 49%), with OL-1 clustering closer to the pIC+R848 group than OL-2 (Figure 5A). The PCA of the DC data showed a similar pattern (Figure 5B); however, in the DC data, PC1 mainly captured the spread of treatment and accounted for a higher amount of variance than in Mf (68 vs 49%), suggesting a larger

treatment effect on the transcriptome. In addition, pIC+R848 clustered separately from the control and the probiotic consortia. Overall, in Mf and DC datasets, OL-1 and OL-2 clustered with pIC+R848 and separate from the controls, indicating a potentially general similarity in immune gene activation. PC loadings for OL-1 Mf samples showed major influence by *IL1B*, *CXCL8*, *CXCL1*, *CXCL2*, *PPBP* (CXCL7), and *TNFAIP6* on the PC1 (Figure 5C). Of these, *IL1B*, *CXCL8,* and *TNFAIP6* were shared with OL-2, whereas *CCL4L2* and *CXCL10* were unique (Figure 5D). The results suggest that the key effects of the consortia versus control are on early innate and chemokine response. For DCs, OL-1 PCA showed separation of OL-1 from the control on PC1 with *IFI6*, *CLEC2D*, *SIGLEC6*, and *CLC* driving the effect (Figure 5E). Of these, *IFI6* and *CLC* were shared with OL-2, whereas *IL15RA*, *HESX1*, *ISG20,* and *GBP4* were unique (Figure 5F). *GBP4, IFI6, ISG20, and CLEC2D* genes are inducible by IFNs, and further *CLC* (Galectin-10) and *CLEC2D* (LLT1) expression by DCs are associated with modulating B and T cell responses.

In differential gene expression (DEG) analysis, OL-1 and OL-2 were compared to control and pIC+R848 to DMSO. In Mfs, OL-1, OL-2, and pIC+R848 treatments resulted in 158, 523, and 1264 DEGs, respectively, whereas in the DCs, OL-1, OL-2, and pIC+R848 treatments resulted in 501, 1264, 670 DEGs, respectively (Table S1 Differentially expressed genes of significance, Figure 5). The number of shared DEGs between OL-1, OL-2, and pIC+R848 was 1350 for Mfs and 596 for DCs. OL-1 and OL-2 treatments shared 308 DEGs in DCs and 184 in Mfs, with pIC+R848 having 1904 unique DEGs in DCs and 184 in Mfs. Overall, the results support the observed increase in cytokine production and cell stimulation by OL-1 and OL-2 and similarity with pIC+R848 stimulation (Figure 4).

We further investigated the effect of the OL-1 and OL-2 on the cytokine, chemokine, and co-stimulatory molecule gene expression. Overall, the profiles of OL-1 and OL-2 were similar except for downregulation (*e.g., IL2, IL7, IL27, and IL36G*) or upregulation (*e.g., IL6, IL32, and TNFA*) of some transcripts in Mfs by OL-2 (Figure 6). Specifically, for Mfs, OL-1 and OL-2 stimulation upregulated most prominently *EBI3* (IL27B), *IL1A*, *IL1B*, *IL12B,* and *IL23A*, necessary for type I immunity. Accordingly, chemokines profiles in Mfs showed broad activation of CCL and CXCL class chemokines, especially CCL1, CCL3, CCL4, CCL15, CXCL1, CXCL2, CXCL8, and CXCL10 that target neutrophils, Mfs, and NK cells. In addition, OL-1 and OL-2 induced HLA and co-stimulatory molecule expression, in line with innate response stimulation, but also upregulated inhibitory CD274 (Figure 6). In DCs, OL-1 and OL-2 induced upregulation of *IL2, IL15, IL18,* and *IL23* that are associated with T cell survival. Furthermore, treatments increased chemokine CX3CL1, CXCL9, CXCL10, CXCL11, CCL17, and CCL22 expression that are associated with attraction and activation of T cells. Probiotic consortia further inhibited CCL2, CCL3, and CCL4 expression that attract CCR2 and CCR5 positive cells such as innate NK cells and monocytes. Co-stimulatory gene expression results showed that DCs upregulated co-stimulatory genes CD80, CD83, CD86 after OL-1 or OL-2 treatment. Interestingly, inhibitory PD-ligands (CD274, PDCD1LG2) were upregulated but on the other hand tolerogenic response-associated CD31 (Clement et al., 2014) and CD36 (Lee et al., 2021) were downregulated. DCs showed upregulation of HLA class I and downregulation of HLA class II genes (Figure 6).

OL-1 and OL-2 perturb COVID-19 KEGG pathway in human macrophages and dendritic cells

SARS-CoV-2 is known to suppress host cells' antiviral mechanisms to enable replication. As we had observed immune stimulation by OL-1 and OL-2, we wanted to further understand the effect of the consortia to antiviral pathways critical for SARS-CoV-2 defense. We conducted pathway analysis using differential expression data which takes into account log2 fold changes and p values for all genes in our dataset and calculates a probability of a KEGG pathway to be perturbed. Overall, OL-1, OL-2, and pIC+R848 affected 81, 36, and, 87 pathways in the Mfs and 71, 79, and 105 pathways in DCs, respectively (adjusted p value < 0.1, FDR) (Table S2 Pathway analysis. Figure 7). Pathways involving viral infections, microbial recognition, and innate and adaptive immune cell signaling pathway activation were broadly perturbed Table S2 Pathway analysis. Figure 7), indicating a general and broad impact by both OL-1 and OL-2 on key human immune defense pathways. In Mfs, OL-2 stimulated less pathways than OL-1, indicating perhaps milder stimulation that would be in line with lower cytokine concentrations in Mfs (Figure 4).

The results of the pathway analysis showed that OL-1 and pIC+R848 resulted in a significant perturbation of the COVID-19 KEGG pathway (KEGG: hsa05171), in Mfs ($p = 0.03$ (OL-1), $p = 0.10$ (OL-2), $p = 0.35$ (pIC+R848), and DCs, ($p = 0.23$ (OL-1), $p = 0.15$ (OL-2), $p = 0.0005$ (pIC+R848)), respectively (Figure 7). The "Coronavirus disease – COVID-19" KEGG pathway consists of 205 genes and includes all stages of viral infection, replication, release, and the SARS-CoV-2-induced innate immune and complement activation. In

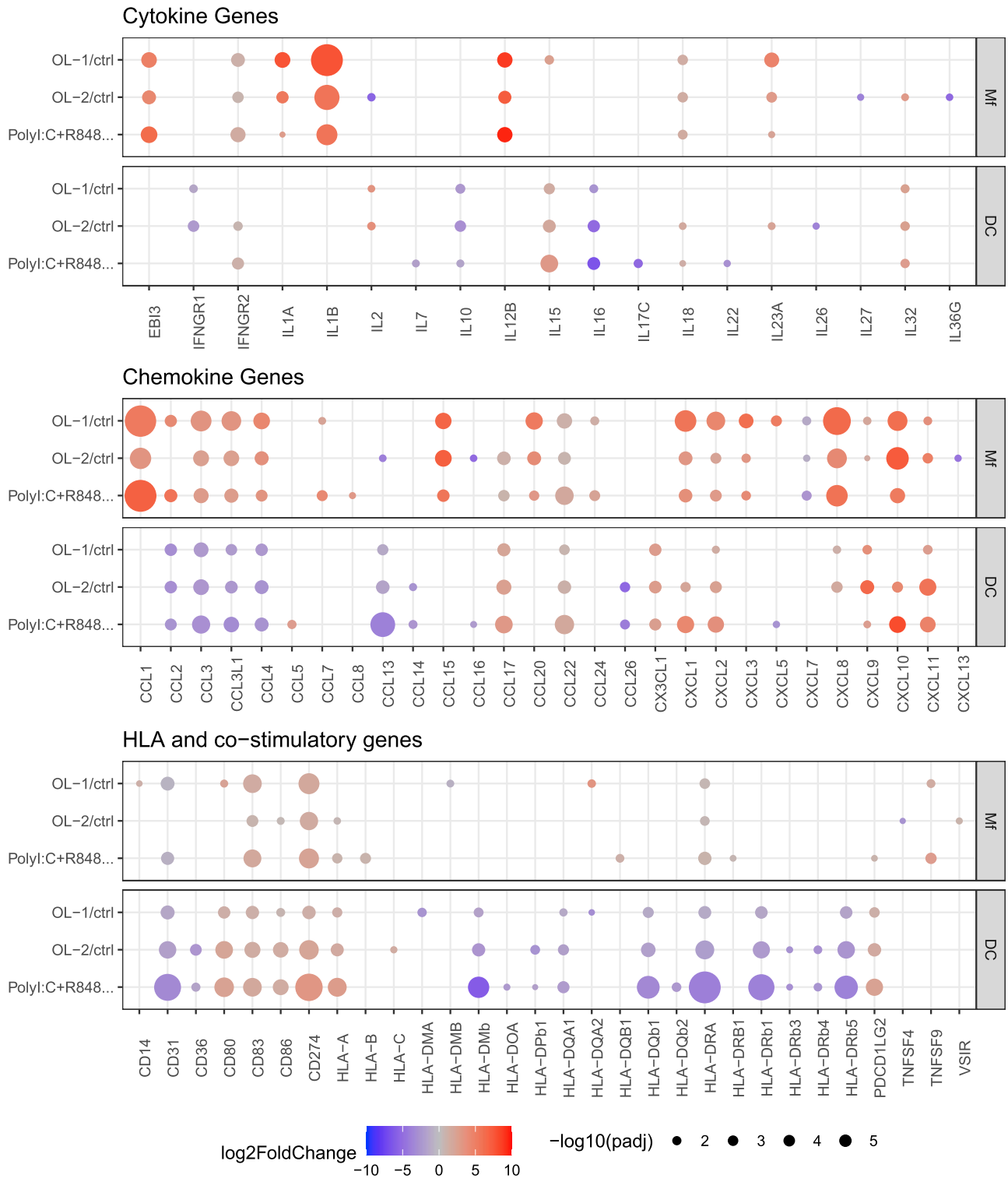

Figure 6. The effect of the OL-1, OL-2, and pIC+R848 on selected cytokines, chemokines, and HLA/co-stimulatory gene response

Balloon plot of selected genes of importance from cytokines, chemokines, and HLA/co-stimulatory gene groups. Only genes that show significant expression (padj <0.10) in either Mf or DC are shown. Size of the balloon denotes significance (-log10 adjusted p value) with the larger size having more significance. Color denotes expression level (log2 fold change) with blue having reduced expression compared to the control and red having increased. Cell type is split in each panel denoted by Mf and DC.

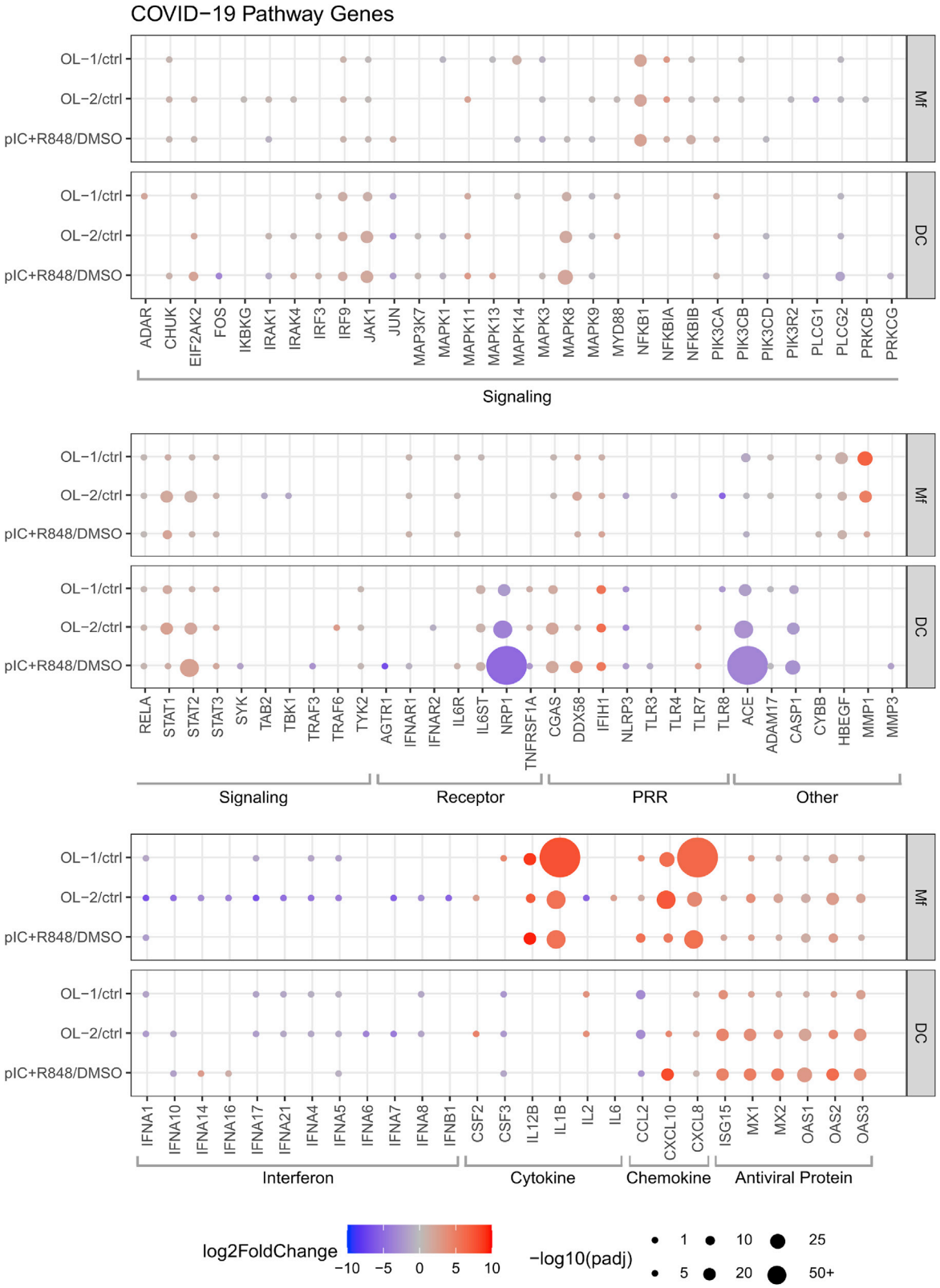
COVID−19 Pathway Genes
OL−1/ctrl
OL−2/ctrl
pIC+R848/DMSO
Mf
DC
ADAR
CHUK
EIF2AK2
FOS
IKBKG
IRAK1
IRAK4
IRF3
IRF9
JAK1
JUN
MAP3K7
MAPK1
MAPK11
MAPK13
MAPK14
MAPK3
MAPK8
MAPK9
MYD88
NFKB1
NFKBIA
NFKBIB
PIK3CA
PIK3CB
PIK3CD
PIK3R2
PLCG1
PLCG2
PRKCB
PRKCG
Signaling
RELA
STAT1
STAT2
STAT3
SYK
TAB2
TBK1
TRAF3
TRAF6
TYK2
AGTR1
IFNAR1
IFNAR2
IL6R
IL6ST
NRP1
TNFRSF1A
CGAS
DDX58
IFIH1
NLRP3
TLR3
TLR4
TLR7
TLR8
ACE
ADAM17
CASP1
CYBB
HBEGF
MMP1
MMP3
Signaling
Receptor
PRR
Other
IFNA1
IFNA10
IFNA14
IFNA16
IFNA17
IFNA21
IFNA4
IFNA5
IFNA6
IFNA7
IFNA8
IFNB1
CSF2
CSF3
IL12B
IL1B
IL2
IL6
CCL2
CXCL10
CXCL8
ISG15
MX1
MX2
OAS1
OAS2
OAS3
Interferon
Cytokine
Chemokine
Antiviral Protein
log2FoldChange
−10 −5 0 5 10
−log10(padj)
1 10 25
5 20 50+

Figure 7. COVID-19 pathway gene expression for OL-1, OL-2, and pIC+R848

Balloon plot of expression of genes taken from the Coronavirus disease – COVID-19 pathway in both Mf and DC cells. Only genes that have an adjusted p value < 0.1 (-log10 > 1) in either Mf or DC are shown. Size of the balloon denotes the log base 10 of the adjusted p value, with smaller p values having larger balloons. Color denotes expression level with blue having reduced expression compared to the control and red having increased. Black bars under the genes denote the function of the set of genes within the pathway. Cell type is split in each panel denoted by Mf and DC.

general, the gene expression pattern showed cell type specific gene expression regulation between Mf and DC after OL-1, OL-2, and pIC+R848 stimulation (Figure 7).

In Mfs and in response to OL-1 and OL-2, interleukin *IL12B* and *IL1B* and chemokine *CXCL10* and *CXCL8* genes were highly expressed compared to low or no induction in DCs (Figure 7). However, the antiviral genes *MX1* and *MX2, OAS1, OAS2, OAS3,* and *ISG15* were strongly induced in DCs and to a somewhat lower extent in Mfs. Interestingly, in DCs, the neuropilin 1 receptor gene NRP1 involved in SARS-CoV-2 entry (Cantuti-Castelvetri et al., 2020) was reduced by all the treatments, as well as the gene coding ACE, whereas *IFIH1* gene coding for MDA5 receptor was upregulated. Monocyte-derived innate immune cells seem to express the genes for SARS-CoV-2 receptor ACE2 and TMPRSS2 protease (Yang et al., 2020) that is needed for the activation of the viral spike protein and facilitation of the virus entry into the cell, but we did not observe these genes to be regulated by the treatments. Matrix metalloproteinase 1 gene (*MMP1)* expression was seen only in Mfs and the expression was higher in OL-1 stimulated cells compared to the others. Many of the JAK-STAT signaling pathway genes were upregulated (Figure 7), especially in DCs, indicating that the probiotic and pIC+R848 activate IFN and ISG production in these cells.

DISCUSSION

The potential of probiotics to support immune function against SARS-CoV-2 is yet to be established. In this study, we have shown the effect of two probiotic consortia OL-1 and OL-2 on reducing nasal wash viral load in a ferret SARS-CoV-2 challenge model. The consortia modulated cytokine, chemokine, and IFN gene expression profiles in lungs and duodenum, suggesting innate immune stimulation by OL-1 and OL-2. In the human monocyte-derived Mf and DC model, we further show that both consortia stimulate Th1 type cytokines and activate IFN response transcriptomic pathways, critical for innate defense against SARS-CoV-2. Besides, the data suggests that the consortia modulates main receptor ACE2 in ferrets and may modulate co-receptors for viral entry in humans.

Probiotics decrease SARS-CoV-2 nasal wash viral load

We evaluated the effect of OL-1 and OL-2 consortia in a pilot and main study on SARS-CoV-2 challenge. The results show a decrease in nasal wash viral load in the main study by both OL-1 and OL-2 probiotic consortia (Figure 1). In the main study, the time course and the magnitude of the SARS-CoV-2 viral titers in the placebo group was comparable to a recent SARS-CoV-2 dose response study in ferrets (Ryan et al., 2021), where the authors were using high (5×10^6 plaque forming units (pfu)/mL), medium (5×10^4 pfu/mL), and low challenge dose (5×10^2 pfu/mL), of which the medium dose is comparable to 10^5 TCID50 target dose in our study. Ryan et al. showed around 10^7 viral RNA copies/mL in the peak replication at 3 days with the high dose, whereas our lower viral dose resulted in an average of 4.9×10^7 genomes/mL (4.9×10^4 genomes/uL) in the placebo group (Figure 1). They further showed that the initial viral inoculum plays a role in subsequent viral load. This indicates potential issues in the viral inoculum of our pilot study that was hampered by low infectivity of ferrets and low viral titers (Figure S1). The low infectivity was also apparent in the very mild immune response of the ferrets to the virus (Figure S2A), and as such, the results of the main study are a better representation of the course of infection and immune response in ferrets as well as the effect of OL-1 and OL-2.

Although ferrets have been recognized as a good model for coronavirus infections, there are very few studies in ferrets where probiotics have been evaluated. Recently, a study assessed the effect of probiotic consortia in ferrets and showed results on behavioral phenotypes after maternal pIC immune activation (Dugyala et al., 2020). However in mice models, probiotics administration has been shown to reduce viral load against influenza and some other respiratory pathogens (Lehtoranta et al., 2020), and in humans, *B. lactis* BI-04 (in consortia OL-1) supplementation was shown to decrease nasal wash viral titers in a rhinovirus challenge model (Turner et al., 2017) and risks of cold in healthy active adults (West et al., 2014). Our study results support the use of ferrets for evaluating the probiotic or microbial therapies efficacy against viral infections.

Probiotic consortia modulate duodenal ACE2 and immune function

ACE2 is the main receptor for the SARS CoV-2, and it has been suggested that decreasing expression could limit viral entry into the cells, but studies on intestinal ACE2 are limited. It has been postulated that there is a potential intestinal infection and fecal-oral transmission of SARS-CoV-2 (Guo et al., 2021). In the gut, ACE2 acts as a key regulator of dietary amino acid homeostasis, innate immunity, gut microbial ecology, and susceptibility to develop inflammation in a RAS-independent manner (Hashimoto et al., 2012). In the current study on D5, during the acute infection, we observed by immunohistology a significantly higher expression of ACE2 in the duodenums of OL-1 and OL-2 group ferrets compared to placebo group animals (Figure 3), but by qPCR lower expression of ACE2 in all groups compared to D0 in the main study (Figure S2B). As it has been shown that SARS-CoV-2 infection decreases ACE2 on the cell membrane (Verdecchia et al., 2020), the results suggest that OL-1 and OL-2 groups may have had lower duodenal viral infection and replication compared to placebo. This hypothesis is supported by increased *IFNA* expression by OL-1 and OL-2 compared to placebo at D5 (Figure 2) and suggests activation of the type I IFN pathway in the gut. On the other hand, ACE2 also acts as the SARS-CoV-2 receptor; in addition, higher ACE2 expression has cytoprotective effects (Gheblawi et al., 2020), and thus the optimal level of ACE2 expression is not clearly known yet (Chaudhry et al., 2020). Despite increase in ACE2, we did not observe differences in the duodenal tissue inflammation (Figure 2) or in inflammatory gene expression response between the treatments at D5 (Figure 3). Interestingly, the Mf and DC treatment with OL-1 and OL-2 decreased expression of *ACE* (Figure 7) that has opposite function to *ACE2*. The results indicate that the effect of the probiotic consortia on the gut ACE-ACE2 balance and RAS system could be cytoprotective. The transcriptomics data also showed a decreased expression of *NRP1* that acts as a cofactor for ACE2-mediated viral cell entry (Figure 7) (Cantuti-Castelvetri et al., 2020), which adds to the evidence on the influence of the OL-1 and OL-2 on SARS-CoV-2 receptors *in vivo and in vitro*.

At D10 in the main study, duodenal ACE2 expression decreased in OL-1 and OL-2 groups compared to placebo, and also compared to D5 OL-1 and OL-2 levels (Figure 3), perhaps suggesting faster resolution to baseline ACE2 expression in probiotic groups; however, with lack of noninfectious samples for baseline, this hypothesis remains to be tested.

The inflammatory gene expression at D10 was comparable to D5 in all groups; however, the histological inflammatory scoring showed a decrease from D5 to D10 (Figures 3I and 3J), in line with resolution of intestinal infection. The effects of OL-1 and OL-2 compared to placebo were relatively pronounced and consistent with duodenal gene expression. Both consortia increased the expression of type III IFN *IFNL1*, monocyte (*CCL2*) and neutrophil (IL8) targeting chemokines, and *TLR8* that recognizes SARS-CoV-2, suggesting stimulation of anti-SARS-CoV-2 immunity. OL-2 also induced cytosolic SARS-CoV-2 pattern recognition receptor *IFIH1* (MDA5), *IL6*, and *TNFA*, and OL-1 decreased *IFNG*, which points to consortia-specific differences on immune stimulation. The differences between OL-1 and OL-2 were also observed in duodenal gene expression in the pilot study, where OL-2 decreased IFN responses at D5, and OL-1 decreased pro-inflammatory and IFN gene expression at D21 compared to placebo. In addition, OL-1 and OL-2 showed significant reduction in ACE2 transcripts when compared to placebo at D21.

So far, little has been done to evaluate therapies or intervention to target the gastrointestinal tract pool of SARS-CoV-2. Based on the differential expression of ACE2 in the duodenum, we propose that OL-1 and OL-2 intervention could potentially be effective in managing the SARS-CoV-2 load in the duodenum, potentially also in humans as supported by decreased expression of *NRP1* and *ACE* in human DC model.

Probiotic delivery by gavage may stimulate gut-lung immune axis

In COVID-19, human lungs are the key site for pathology and viral replication and thus ferret lung immune response modulation could be of relevance, although SARS-CoV-2 is mostly upper respiratory infection in ferrets (Munoz-Fontela et al., 2020). The gene expression results at D5 and D10 of the main study compared to noninfected ferrets from the pilot study show that SARS-CoV-2 induces type I (*IFNA*) and III (*IFNL1*) IFN responses, but suppresses type II response (*IFNG*), and stimulates pro-inflammatory (*IL6* and *IL8*) and anti-inflammatory (*IL10*) gene expression (Figure S2B). Overall, the cytokine profiles indicate balanced response of the ferrets to the virus where the viral replication is controlled without cytokine storm. We also observed at D5 and D10 in all groups and increased expression of *ACE2* that has anti-inflammatory and cytoprotective properties in addition to its role as a receptor for SARS-CoV-2 (Gheblawi et al., 2020). The aforementioned results are in line with the lack of symptoms in the ferrets and low viral load by D10 (Figure 1). In the

pilot study, minimal changes in gene expression were observed that likely reflects the low infectivity (Figures S1 and S2). Similar immune responses in ferrets to SARS-CoV-2 — as in the main study — have been observed previously (Blanco-Melo et al., 2020), which supports our use of noninfected placebo treated animals from the pilot study to normalize the response of the infection in the main study (Figure S2B); however, the results need to be interpreted cautiously.

Probiotic effect compared to placebo on the lung gene expression was low. In the main study, at D5, OL-2 increased expression of chemokines (*CXCL10* and *IL8*), targeting NK cells and neutrophils, and *TLR8* that recognizes viral RNA (Figure 2). This effect was not observed at D10 and could be because of resolution of the infection. In the pilot study, OL-1 at D0 decreased *CXCL10* and *TLR8*, suggesting effects on the lung immune function preinfection; however, no changes were observed in duodenum. At D5, OL-1 increased *IFNG*, and at D21 postinfection, the differences were most pronounced for OL-1 that increased *IFNA, IFNL1, IL10, IL6*, and *TNFA* and decreased *CCL2*, also suggesting effects postinfection. In summary, probiotic consortia seem to induce lung immune system, but the effects seem mild and somewhat inconsistent in this dataset. On the other hand, OL-1 and OL-2 reduced the viral load that is suggestive of influence on the nasal immune system as well. The effect of the probiotic consortia on gut-lung or gut-respiratory axis warrants further investigation.

OL-1 and OL-2 may prime innate immune responses against viral infections

Innate immune systems between ferrets and humans, and mammals in general are homologous; however, to gain further understanding on potential effect of the consortia in humans, we exposed human blood-derived Mfs and DCs to OL-1 and OL-2 and viral RNA analog cocktail pIC+R848 and analyzed their cytokine and transcriptome responses.

The studies on SARS-CoV-2 infection and pathogenesis indicate that inadequate innate immune and IFN response increase susceptibility to more severe COVID-19 (Schultze and Aschenbrenner, 2021) that is supported by increased risk of more severe disease by aging. Our results show that exposure of Mfs to OL-1 and OL-2 resulted in the secretion of cytokines important for Mf activation and induction of type I immunity (IL-12 and IFN-γ), but also drove pro-inflammatory and anti-inflammatory cytokine production (Figure 4). These results were supported by transcriptomics analysis showing activation of IL-1 and IL-12 cytokine family genes, upregulation of co-stimulatory molecules, MHC-I/II and chemokines targeting monocytes, NK cells, and neutrophils critical for early defense in viral infections (Figure 6). DC response to OL-1 and OL-2 further show Th1 polarization as determined by increased IL-12p70 production (Figure 4). The transcriptomics analysis further showed an increase in STAT1 (Figure 7) that drives in DCs Th1 polarization (Johnson and Scott, 2007), induction of co-stimulatory and MHC-I molecules, and upregulation of genes related to T cell growth and attraction. Lu et al., (2021) showed that SARS CoV-2 (24 h infection with clinical isolates) induces *IL1A, IL1B, IL8, CXCL10, CCL2,* and *CCL3* mRNA in human PBMC-derived myeloid cells (Lu et al., 2021). We see quite similar gene induction patterns in our monocyte-derived Mfs (Figure 7), where both consortia and pIC+R848 induce some of the same genes as SARS-CoV-2, suggesting induction of antiviral pathways. In summary, the results show that probiotic consortia could prime or train the innate immune system also in humans before SARS-CoV-2 infection to enhance resilience of the host.

Priming of the innate system by OL-1 or OL-2 is a potential mechanism to explain the reduced viral load that we observed in the ferrets after 7 days of supplementation (Figure 1). Although we have limited data preinfection, the postinfection gene expression results suggest enhanced response in duodenum, but also potentially in lungs (Figure 2). Netea et al. have suggested that the training of the human innate immune system, for example by vaccines, before SARS-CoV-2 infection could reduce the susceptibility to and the risk of severe COVID-19 (Netea et al., 2020). Similar evidence on priming of the immune system against viral infections by probiotics has been noted more broadly *in vitro* and in human clinicals (Lehtoranta et al., 2020; Turner et al., 2017).

Probiotic consortia may counteract SARS-CoV-2 immune-evasion

Studies on the early pathogenesis of SARS-CoV-2 show that it infects the cells via ACE2 that is internalized. The host cells recognize the virus by endosomal (TLR3, TLR7, and TLR8) and cytosolic (RIG-I and MDA5) receptors that recognize ssRNA and dsRNA. This leads to an MyD88 and NF-κB -dependent activation of pro-inflammatory response and IRF3/7 -dependent type I IFN response. IFNs drive STAT1/2 and IRF9-mediated ISG response. SARS-CoV-2 produces proteins that suppress the activation of this cascade (Schultze and

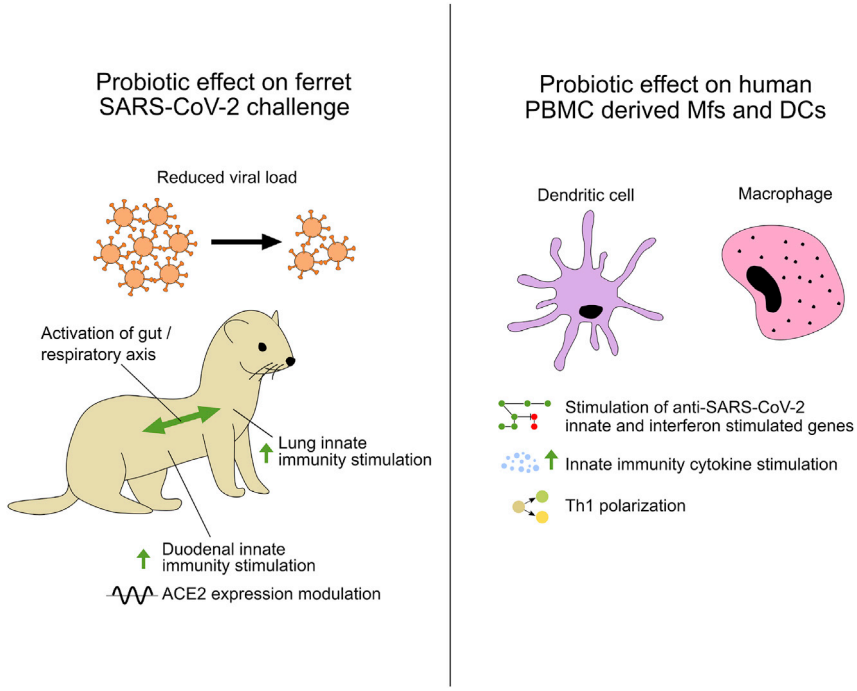

Figure 8. Summary of the effect of the probiotic consortia in ferrets on SARS-CoV-2 challenge and human Mfs and DCs

Probiotic gavage of OL-1 and OL-2 stimulate ferret duodenal and respiratory tract innate immunity and reduce SARS-CoV-2 viral load in nasal washes, thus suggesting activation of gut-respiratory axis immunity. Besides, Mf and DC stimulation by OL-1 and OL-2 show activation of critical genes and secretion of cytokines important for anti-SARS-CoV-2 innate immunity, suggesting that these probiotic consortia could also be beneficial in humans.

Aschenbrenner, 2021). The results of our transcriptomics study show that OL-1 can significantly modulate the KEGG COVID-19 pathway in Mfs, and that OL-2 shows a similar gene expression pattern in Mfs but does not result in a significant change on a pathway level (Figure 7). In DCs, the result on a pathway level is significant only for pIC+R848; however, OL-1 and OL-2 show similar patterns of significant gene expression (Figure 7). Several signaling molecules on the pathways in Mfs and DCs show upregulation by the consortia including *IRF3, IRF9, NFKB1, STAT1, STAT2*, and ISGs *ISG15, MX1, MX2, OAS1, OAS2, OAS3,* and *CGAS*. In addition, viral RNA sensors *IFIH1* (MDA5) and *DDX58* (RIG-I) show an increased expression, whereas *TLR7* and *TLR8* expression have mixed results. Interestingly, type I IFN family gene expression seems to be suppressed or unimpacted by OL-1 and OL-2 but mainly also by pIC+R848 (Figure 7). Overall, the results suggest that OL-1 especially, but also OL-2, could potentially counteract suppression of the innate immune system activation by SARS-CoV-2. Delayed or poor IFN response has been associated with more severe COVID-19 disease in human clinical samples (Hadjadj et al., 2020) and lower levels of pro-inflammatory cytokines and chemokines noted with SARS-CoV-2 infection (Blanco-Melo et al., 2020; Chu et al., 2020), suggesting that targeting innate immunity with probiotic consortia could provide benefits in managing SARS-CoV-2 infection in humans; however, making conclusions on efficacy of probiotics in humans requires clinical data.

Conclusions

In this study, we have shown that probiotic consortia OL-1 and OL-2 stimulate ferret immune function and reduce viral load during SARS-CoV-2 infection (Figure 8). Results of the human immune cell stimulation indicate that pathways and cytokine secretion associated with SARS-CoV-2 immune defense are activated, and thus these probiotic consortia could potentially provide benefits to support immune function against SARS-CoV-2, perhaps by priming or training the innate immune system (Lehtoranta et al., 2020; Netea et al., 2020) (Figure 8). We have also shown the influence of the probiotic consortia on duodenal immune function and ACE2 expression. As many COVID-19 patients suffer from gastrointestinal symptoms, these probiotic consortia could potentially support intestinal health and immune function. Probiotics in general

have shown efficacy in meta-analyses against respiratory tract infections (Hao et al., 2015; King et al., 2014); however, the results between the strains or their combinations vary. Thus, it is warranted to use specific strains or consortia of probiotics for immune stimulation (Hill et al., 2014). Even small differences in genome or within strains may result in vast differences in phenotypes and metabolism (Morovic et al., 2018; Zabel et al., 2020). Human clinical studies should be conducted to better understand the effect of OL-1 and OL-2, and other microbial therapies in managing SARS-CoV-2 infections.

Limitations of the study

We have discussed the limitations of the study broadly in the discussion; however, it is noteworthy to highlight here that in the ferret study, the results between the main and the pilot studies were somewhat conflicting, justifying further investigations into the effect of probiotics on immune function and anti-SARS-CoV-2 immunity. In addition, we did not specifically study the colonization of the probiotics or their effect on the microbiota in this study. The *in vivo* and human macrophage and dendritic cell studies would have benefited on inclusion of non-probiotic bacteria or other well-studied probiotic strains to better evaluate the effect size and specificity of the immune response to OL-1 and OL-2 consortia.

STAR★METHODS

Detailed methods are provided in the online version of this paper and include the following:

- KEY RESOURCES TABLE
- RESOURCE AVAILABILITY
  - Lead contact
  - Materials availability
  - Data and code availability
- EXPERIMENTAL MODEL AND SUBJECT DETAILS
  - Probiotic strains and placebo
  - Ferrets
  - Human PBMC derived macrophages and dendritic cells
- METHOD DETAILS
  - Ferret studies
  - RT-qPCR SARS-CoV-2 titers
  - Gene expression analysis by qPCR
  - Immunohistochemical analysis of duodenum for ACE2 expression
  - Cell stimulation assay
  - Enzyme linked immunosorbent assay
  - RNA extraction
  - Transcriptomics
- QUANTIFICATION AND STATISTICAL ANALYSIS
  - Viral titer analysis
  - Quantitative PCR
  - Histopathological examination of duodenum
  - Enzyme linked immunosorbent analysis
  - Transcriptomics

SUPPLEMENTAL INFORMATION

Supplemental information can be found online at https://doi.org/10.1016/j.isci.2022.104445.

ACKNOWLEDGMENTS

Jaana Larsson-Leskelä, Katri Holappa, Henri Ahokoski, Anna Lappalainen for excellent technical work, and Ilmari Ahonen, PhD; Senior Data Scientist, Vincit Plc for statistical analysis of the ELISA data. Xinjian Peng, PhD; Senior Biologist, IIT Research Institute (IITRI).

AUTHOR CONTRIBUTIONS

Conceptualization, M.J.L., S.G., R.K., B.Z., and C.R.B.; Data curation, B.Z., D.N., and P.T.; Formal analysis, B.Z., D.N., and P.T.; Funding Acquisition, S.G.; Investigation, M.J.L., S.L., R.K., and B.Z.; Methodology, B.Z., D.N., and P.T.; Project Administration, M.J.L.; Software, B.Z., D.N., and P.T.; Supervision, M.J.L., S.G., R.K.,

and C.R.B.; Visualization, M.J.L., R.K., B.Z., D.N., and P.T.; Writing – Original Draft, M.J.L., S.M.M., R.K., B.Z., and P.T.; Writing – Review & Editing, M.J.L., S.M.M., S.L., R.K., B.Z., D.N., P.T., S.G., and C.R.B.

DECLARATION OF INTERESTS

M.J.L., R.K., S.L., C.R.B., and S.G. have filed a patent under the provisional series. All authors are employees of IFF that manufactures and sells probiotics used in the study.

Received: August 30, 2021
Revised: November 19, 2021
Accepted: May 18, 2022
Published: June 17, 2022

REFERENCES

Alfi, O., Yakirevitch, A., Wald, O., Wandel, O., Izhar, U., Oiknine-Djian, E., Nevo, Y., Elgavish, S., Dagan, E., Madgar, O., et al. (2021). Human nasal and lung tissues infected ex vivo with SARS-CoV-2 provide insights into differential tissue-specific and virus-specific innate immune responses in the upper and lower respiratory tract. J. Virol. *95*. e00130-00121. https://doi.org/10.1128/jvi.00130-21.

Blanco-Melo, D., Nilsson-Payant, B.E., Liu, W.C., Uhl, S., Hoagland, D., Moller, R., Jordan, T.X., Oishi, K., Panis, M., Sachs, D., et al. (2020). Imbalanced host response to SARS-CoV-2 drives development of COVID-19. Cell *181*, 1036–1045.e9. https://doi.org/10.1016/j.cell.2020.04.026.

Cantuti-Castelvetri, L., Ojha, R., Pedro, L.D., Djannatian, M., Franz, J., Kuivanen, S., van der Meer, F., Kallio, K., Kaya, T., Anastasina, M., et al. (2020). Neuropilin-1 facilitates SARS-CoV-2 cell entry and infectivity. Science *370*, 856–860. https://doi.org/10.1126/science.abd2985.

Chaudhry, F., Lavandero, S., Xie, X., Sabharwal, B., Zheng, Y.Y., Correa, A., Narula, J., and Levy, P. (2020). Manipulation of ACE2 expression in COVID-19. Open Heart *7*, e001424. https://doi.org/10.1136/openhrt-2020-001424.

Chu, H., Chan, J.F., Wang, Y., Yuen, T.T.T., Yuen, T.T., Chai, Y., Hou, Y., Shuai, H., Yang, D., Hu, B., et al. (2020). Comparative replication and immune activation profiles of SARS-CoV-2 and SARS-CoV in human lungs: an ex vivo study with implications for the pathogenesis of COVID-19. Clin. Infect. Dis. *71*, 1400–1409. https://doi.org/10.1093/cid/ciaa410.

Clement, M., Fornasa, G., Guedj, K., Ben Mkaddem, S., Gaston, A.T., Khallou-Laschet, J., Morvan, M., Nicoletti, A., and Caligiuri, G. (2014). CD31 is a key coinhibitory receptor in the development of immunogenic dendritic cells. Proc. Natl. Acad. Sci. U. S. A *111*, E1101–E1110. https://doi.org/10.1073/pnas.1314505111.

Dugyala, S., Ptacek, T.S., Simon, J.M., Li, Y., and Frohlich, F. (2020). Putative modulation of the gut microbiome by probiotics enhances preference for novelty in a preliminary double-blind placebo-controlled study in ferrets. Anim. Microbiome *2*, 14. https://doi.org/10.1186/s42523-020-00030-y.

Gheblawi, M., Wang, K., Viveiros, A., Nguyen, Q., Zhong, J.C., Turner, A.J., Raizada, M.K., Grant, M.B., and Oudit, G.Y. (2020). Angiotensin-converting enzyme 2: SARS-CoV-2 receptor and regulator of the renin-angiotensin system: celebrating the 20th anniversary of the discovery of ACE2. Circ. Res. *126*, 1456–1474. https://doi.org/10.1161/circresaha.120.317015.

Guo, M., Tao, W., Flavell, R.A., and Zhu, S. (2021). Potential intestinal infection and faecal-oral transmission of SARS-CoV-2. Nat. Rev. Gastroenterol. Hepatol. *18*, 269–283. https://doi.org/10.1038/s41575-021-00416-6.

Hadjadj, J., Yatim, N., Barnabei, L., Corneau, A., Boussier, J., Smith, N., Péré, H., Charbit, B., Bondet, V., Chenevier-Gobeaux, C., et al. (2020). Impaired type I interferon activity and inflammatory responses in severe COVID-19 patients. Science *369*, 718–724. https://doi.org/10.1126/science.abc6027.

Hao, Q., Dong, B.R., and Wu, T. (2015). Probiotics for preventing acute upper respiratory tract infections. Cochrane Database Syst. Rev. Cd006895. https://doi.org/10.1002/14651858.cd006895.pub3.

Harper, A., Vijayakumar, V., Ouwehand, A.C., ter Haar, J., Obis, D., Espadaler, J., Binda, S., Desiraju, S., and Day, R. (2021). Viral infections, the microbiome, and probiotics. Front. Cell. Infect. Microbiol. *10*, 596166. https://doi.org/10.3389/fcimb.2020.596166.

Hashimoto, T., Perlot, T., Rehman, A., Trichereau, J., Ishiguro, H., Paolino, M., Sigl, V., Hanada, T., Hanada, R., Lipinski, S., et al. (2012). ACE2 links amino acid malnutrition to microbial ecology and intestinal inflammation. Nature *487*, 477–481. https://doi.org/10.1038/nature11228.

Hill, C., Guarner, F., Reid, G., Gibson, G.R., Merenstein, D.J., Pot, B., Morelli, L., Canani, R.B., Flint, H.J., Salminen, S., et al. (2014). Expert consensus document. The International Scientific Association for Probiotics and Prebiotics consensus statement on the scope and appropriate use of the term probiotic. Nat. Rev. Gastroenterol. Hepatol. *11*, 506–514. https://doi.org/10.1038/nrgastro.2014.66.

Hoagland, D.A., Moller, R., Uhl, S.A., Oishi, K., Frere, J., Golynker, I., Horiuchi, S., Panis, M., Blanco-Melo, D., Sachs, D., et al. (2021). Leveraging the antiviral type I interferon system as a first line of defense against SARS-CoV-2 pathogenicity. Immunity *54*, 557–570.e5. https://doi.org/10.1016/j.immuni.2021.01.017.

Hoffmann, M., Kleine-Weber, H., Schroeder, S., Kruger, N., Herrler, T., Erichsen, S., Schiergens, T.S., Herrler, G., Wu, N.H., Nitsche, A., et al. (2020). SARS-CoV-2 cell entry depends on ACE2 and TMPRSS2 and is blocked by a clinically proven protease inhibitor. Cell *181*, 271–280. https://doi.org/10.1016/j.cell.2020.02.052.

Johnson, L.M., and Scott, P. (2007). STAT1 expression in dendritic cells, but not T cells, is required for immunity to Leishmania major. J. Immunol. *178*, 7259–7266. https://doi.org/10.4049/jimmunol.178.11.7259.

Kanehisa, M. (2019). Toward understanding the origin and evolution of cellular organisms. Protein Sci. *28*, 1947–1951. https://doi.org/10.1002/pro.3715.

Kanehisa, M., Furumichi, M., Sato, Y., Ishiguro-Watanabe, M., and Tanabe, M. (2021). KEGG: integrating viruses and cellular organisms. Nucleic Acids Res. *49*. D545-d551. https://doi.org/10.1093/nar/gkaa970.

Kanehisa, M., and Goto, S. (2000). KEGG: kyoto encyclopedia of genes and genomes. Nucleic Acids Res. *28*, 27–30. https://doi.org/10.1093/nar/28.1.27.

Kim, Y.I., Kim, S.G., Kim, S.M., Kim, E.H., Park, S.J., Yu, K.M., Chang, J.H., Kim, E.J., Lee, S., Casel, M.A.B., et al. (2020). Infection and rapid transmission of SARS-CoV-2 in ferrets. Cell Host Microbe *27*, 704–709. https://doi.org/10.1016/j.chom.2020.03.023.

King, S., Glanville, J., Sanders, M.E., Fitzgerald, A., and Varley, D. (2014). Effectiveness of probiotics on the duration of illness in healthy children and adults who develop common acute respiratory infectious conditions: a systematic review and meta-analysis. Br. J. Nutr. *112*, 41–54. https://doi.org/10.1017/s0007114514000075.

Lee, J.G., Jaeger, K.E., Seki, Y., Wei Lim, Y., Cunha, C., Vuchkovska, A., Nelson, A.J., Nikolai, A., Kim, D., Nishimura, M., et al. (2021). Human CD36(hi) monocytes induce Foxp3(+) CD25(+) T cells with regulatory functions from CD4 and CD8 subsets. Immunology *163*, 293–309. https://doi.org/10.1111/imm.13316.

Lee, S., Channappanavar, R., and Kanneganti, T.D. (2020). Coronaviruses: innate immunity, inflammasome activation, inflammatory cell death, and cytokines. Trends Immunol. *41*, 1083–1099. https://doi.org/10.1016/j.it.2020.10.005.

Lehtoranta, L., Latvala, S., and Lehtinen, M.J. (2020). Role of probiotics in stimulating the immune system in viral respiratory tract

infections: a narrative review. Nutrients *12*, 3163. https://doi.org/10.3390/nu12103163.

Lenth, R.V., Buerkner, P., Herve, M., Love, J., Riebl, H., and Singmann, H. (2021). emmeans: Estimated Marginal Means, aka Least-Squares Means (R package version 1.6.1).

Love, M.I., Huber, W., and Anders, S. (2014). Moderated estimation of fold change and dispersion for RNA-seq data with DESeq2. Genome Biol. *15*, 550. https://doi.org/10.1186/s13059-014-0550-8.

Lu, Q., Liu, J., Zhao, S., Gomez Castro, M.F., Laurent-Rolle, M., Dong, J., Ran, X., Damani-Yokota, P., Tang, H., Karakousi, T., et al. (2021). SARS-CoV-2 exacerbates proinflammatory responses in myeloid cells through C-type lectin receptors and Tweety family member 2. Immunity *54*, 1304–1319.e9. https://doi.org/10.1016/j.immuni.2021.05.006.

Miettinen, M., Pietila, T.E., Kekkonen, R.A., Kankainen, M., Latvala, S., Pirhonen, J., Osterlund, P., Korpela, R., and Julkunen, I. (2012). Nonpathogenic Lactobacillus rhamnosus activates the inflammasome and antiviral responses in human macrophages. Gut Microb. *3*, 510–522. https://doi.org/10.4161/gmic.21736.

Morovic, W., Roos, P., Zabel, B., Hidalgo-Cantabrana, C., Kiefer, A., Barrangou, R., and Müller, V. (2018). Transcriptional and functional analysis of Bifidobacterium animalis subsp. lactis exposure to tetracycline. Appl. Environ. Microbiol. *84*. e01999-01918. https://doi.org/10.1128/aem.01999-18.

Munoz-Fontela, C., Dowling, W.E., Funnell, S.G.P., Gsell, P.S., Riveros-Balta, A.X., Albrecht, R.A., Andersen, H., Baric, R.S., Carroll, M.W., Cavaleri, M., et al. (2020). Animal models for COVID-19. Nature *586*, 509–515. https://doi.org/10.1038/s41586-020-2787-6.

Munshi, I., Khandvilkar, A., Chavan, S., Sachdeva, G., Mahale, S., and Chaudhari, U. (2021). An overview of preclinical animal models for SARS-CoV-2 pathogenicity. Indian J. Med. Res. *153*, 17–25. https://doi.org/10.4103/ijmr.ijmr_3215_20.

Netea, M.G., Giamarellos-Bourboulis, E.J., Dominguez-Andres, J., Curtis, N., van Crevel, R., van de Veerdonk, F.L., and Bonten, M. (2020). Trained immunity: a tool for reducing susceptibility to and the severity of SARS-CoV-2 infection. Cell *181*, 969–977. https://doi.org/10.1016/j.cell.2020.04.042.

Patro, R., Duggal, G., Love, M.I., Irizarry, R.A., and Kingsford, C. (2017). Salmon provides fast and bias-aware quantification of transcript expression. Nat. Methods *14*, 417–419. https://doi.org/10.1038/nmeth.4197.

Peacock, T.P., Goldhill, D.H., Zhou, J., Baillon, L., Frise, R., Swann, O.C., Kugathasan, R., Penn, R., Brown, J.C., Sanchez-David, R.Y., et al. (2021). The furin cleavage site in the SARS-CoV-2 spike protein is required for transmission in ferrets. Nat Microbiol *6*, 899–909. https://doi.org/10.1038/s41564-021-00908-w.

Ryan, K.A., Bewley, K.R., Fotheringham, S.A., Slack, G.S., Brown, P., Hall, Y., Wand, N.I., Marriott, A.C., Cavell, B.E., Tree, J.A., et al. (2021). Dose-dependent response to infection with SARS-CoV-2 in the ferret model and evidence of protective immunity. Nat. Commun. *12*, 81. https://doi.org/10.1038/s41467-020-20439-y.

Salli, K., Hirvonen, J., Siitonen, J., Ahonen, I., Anglenius, H., and Maukonen, J. (2021). Selective utilization of the human milk oligosaccharides 2′-fucosyllactose, 3-fucosyllactose, and difucosyllactose by various probiotic and pathogenic bacteria. J. Agric. Food Chem. *69*, 170–182. https://doi.org/10.1021/acs.jafc.0c06041.

Schultze, J.L., and Aschenbrenner, A.C. (2021). COVID-19 and the human innate immune system. Cell *184*, 1671–1692. https://doi.org/10.1016/j.cell.2021.02.029.

Shi, H.Y., Zhu, X., Li, W.L., Mak, J.W.Y., Wong, S.H., Zhu, S.T., Guo, S.L., Chan, F.K.L., Zhang, S.T., and Ng, S.C. (2021). Modulation of gut microbiota protects against viral respiratory tract infections: a systematic review of animal and clinical studies. Eur. J. Nutr. *60*, 4151–4174. https://doi.org/10.1007/s00394-021-02519-x.

Stanifer, M.L., Kee, C., Cortese, M., Zumaran, C.M., Triana, S., Mukenhirn, M., Kraeusslich, H.G., Alexandrov, T., Bartenschlager, R., and Boulant, S. (2020). Critical role of type III interferon in controlling SARS-CoV-2 infection in human intestinal epithelial cells. Cell Rep. *32*, 107863. https://doi.org/10.1016/j.celrep.2020.107863.

Taefehshokr, N., Taefehshokr, S., Hemmat, N., and Heit, B. (2020). Covid-19: perspectives on innate immune evasion. Front. Immunol. *11*, 580641. https://doi.org/10.3389/fimmu.2020.580641.

Turner, R.B., Woodfolk, J.A., Borish, L., Steinke, J.W., Patrie, J.T., Muehling, L.M., Lahtinen, S., and Lehtinen, M.J. (2017). Effect of probiotic on innate inflammatory response and viral shedding in experimental rhinovirus infection - a randomised controlled trial. Benef. Microbes *8*, 207–215. https://doi.org/10.3920/bm2016.0160.

Verdecchia, P., Cavallini, C., Spanevello, A., and Angeli, F. (2020). The pivotal link between ACE2 deficiency and SARS-CoV-2 infection. Eur. J. Intern. Med. *76*, 14–20. https://doi.org/10.1016/j.ejim.2020.04.037.

Vignesh, R., Swathirajan, C.R., Tun, Z.H., Rameshkumar, M.R., Solomon, S.S., and Balakrishnan, P. (2021). Could perturbation of gut microbiota possibly exacerbate the severity of COVID-19 via cytokine storm? Front. Immunol. *11*, 607734. https://doi.org/10.3389/fimmu.2020.607734.

Voichita, C., Ansari, S., and Draghici, S. (2019). ROntoTools: R Onto-Tools suite. In R package.

Weiss, G., Rasmussen, S., Zeuthen, L.H., Nielsen, B.N., Jarmer, H., Jespersen, L., and Frokiaer, H. (2010). Lactobacillus acidophilus induces virus immune defence genes in murine dendritic cells by a Toll-like receptor-2-dependent mechanism. Immunology *131*, 268–281. https://doi.org/10.1111/j.1365-2567.2010.03301.x.

West, N.P., Horn, P.L., Pyne, D.B., Gebski, V.J., Lahtinen, S.J., Fricker, P.A., and Cripps, A.W. (2014). Probiotic supplementation for respiratory and gastrointestinal illness symptoms in healthy physically active individuals. Clin. Nutr. *33*, 581–587. https://doi.org/10.1016/j.clnu.2013.10.002.

Wickham, H. (2016). ggplot2: Elegant Graphics for Data Analysis (Springer-Verlag).

Yang, D., Chu, H., Hou, Y., Chai, Y., Shuai, H., Lee, A.C.-Y., Zhang, X., Wang, Y., Hu, B., Huang, X., et al. (2020). Attenuated interferon and proinflammatory response in SARS-CoV-2–infected human dendritic cells is associated with viral antagonism of STAT1 phosphorylation. J. Infect. Dis. *222*, 734–745. https://doi.org/10.1093/infdis/jiaa356.

Zabel, B.E., Gerdes, S., Evans, K.C., Nedveck, D., Singles, S.K., Volk, B., and Budinoff, C. (2020). Strain-specific strategies of 2′-fucosyllactose, 3-fucosyllactose, and difucosyllactose assimilation by Bifidobacterium longum subsp. infantis Bi-26 and ATCC 15697. Sci. Rep. *10*, 15919. https://doi.org/10.1038/s41598-020-72792-z.

Zheng, J., Wang, Y., Li, K., Meyerholz, D.K., Allamargot, C., and Perlman, S. (2021). Severe acute respiratory syndrome coronavirus 2-induced immune activation and death of monocyte-derived human macrophages and dendritic cells. J. Infect. Dis. *223*, 785–795. https://doi.org/10.1093/infdis/jiaa753.

Zhou, R., To, K.K., Wong, Y.C., Liu, L., Zhou, B., Li, X., Huang, H., Mo, Y., Luk, T.Y., Lau, T.T.K., et al. (2020a). Acute SARS-CoV-2 infection impairs dendritic cell and T cell responses. Immunity *53*, 864–877.e5. https://doi.org/10.1016/j.immuni.2020.07.026.

Zhou, Z., Ren, L., Zhang, L., Zhong, J., Xiao, Y., Jia, Z., Guo, L., Yang, J., Wang, C., Jiang, S., et al. (2020b). Heightened innate immune responses in the respiratory tract of COVID-19 patients. Cell Host Microbe *27*, 883–890.e2. https://doi.org/10.1016/j.chom.2020.04.017.

STAR★METHODS

KEY RESOURCES TABLE

REAGENT or RESOURCE	SOURCE	IDENTIFIER
Antibodies		
Goat Anti-ACE2 antibody	R&D	Cat#: AF933, Lot#: HOK0620051; RRID: AB_355722
Bacterial and virus strains		
Bifidobacterium longum subsp. *infantis* Bi-26	Danisco Global Culture Collection (DGCC)	(DGCC)11473
Bifidobacterium animalis subsp. *lactis* Bl-04	DGCC, American Type Culture Collection (ATCC)	(SD)5219, DGCC2908
Lacticaseibacillus paracasei subsp. *paracasei* Lpc-37	DGCC, ATCC	SD5275, PTA-4798
Lacticaseibacillus rhamnosus Lr-32	ATCC	SD5217
Ligilactobacillus salivarius Ls-33	ATCC	SD5208
Bifidobacterium animalis subsp. *lactis* Bi-07	ATCC, DGCC	SD5220, DGCC2907
Lactobacillus acidophilus NCFM	ATCC	SD5221, ATCC700396
Limosilactobacillus fermentum SBS-1	DGCC	DGCC1925
Lactococcus lactis subsp. *lactis* Ll-23	DGCC	DGCC8656
Streptococcus thermophilus subsp. *thermophilus* St-21	ATCC	SD5207
2019 Novel Coronavirus isolate	IITRI	USA-WA1/2020
Chemicals, peptides, and recombinant proteins		
TLR ligand R848	Sigma-Aldrich, St. Louis, MO, USA	Product#: SML0196-10MG
TLR ligand PolyI:C	Sigma-Aldrich, St. Louis, MO, USA	Product#: P1530-25MG
Recombinant human GM-CSF, premium grade	Miltenyi Biotec, Auburn, CA, USA	Product#: 130-093-868
Recombinant human IL-4, premium grade	Miltenyi Biotec, Auburn, CA, USA	Product#: 130-093-922
MACS $CD14^+$ beads	Miltenyi Biotec, Auburn, CA, USA	Product#: 130-050-201
Critical commercial assays		
Direct-Zol RNA Miniprep Plus kit	Zymo	Cat#: R2072
iScript Reverse Transcription Supermix	Bio-Rad	Cat#: 1708840
Quanterix Human Corplex Cytokine 7-Plex Array	Quanterix, Billerica, MA, USA	Cat#: 116-6B3-1-AB
Simoa IL-23 Developer Kit	Quanterix, Billerica, MA, USA	Product #: 100-0440
Simoa TGFβ1 Developer Kit	Quanterix, Billerica, MA, USA	Product #: 100-0021
MagMAX™-96 Total RNA Isolation Kit	Invitrogen, Thermo Fisher Scientific	Cat#: AM1830
BioSpyder Whole Human Transcriptomic Kit	Biospyder	https://www.biospyder.com/
Deposited data		
Ferret qPCR data	This Study	GEO#:GSE180390
Macrophage and dendritic cell RNA-seq	This study	GEO#:GSE180389
Experimental models: Organisms/strains		
Outbred male ferrets	Triple F Farms, Sayre, PA	N/A
Human blood monocytes	Finnish Red Cross Blood Service	Permission #: 46/2016
Oligonucleotides		
2019-nCoV_N1-F 5′-GACCCCAAAAT CAGCGAAAT-3′	GenScript	N/A
2019-nCoV_N1-R-5′-TCTGGTTACTG CCAGTTGAATCTG -3′	GenScript	N/A

(*Continued on next page*)

Continued

REAGENT or RESOURCE	SOURCE	IDENTIFIER
Probe:2019-nCoV_N1-P:5′-FAM-ACCCCGCATT ACGTTTGGTGGACC-BHQ1-3′	GenScript	N/A
Primers for gene expression analysis by qPCR found in Table S3	This paper	N/A
Software and algorithms		
CFX Maestro 1.1 software	Bio-Rad	N/A
Olyvia 3.2 software	Olympus Corporation	N/A
CiraSoft software	Quanterix	N/A
Salmon (v1.1.0)	Patro et al. (2017)	
emmeans (v1.6.1)	Lenth et al. (2021)	https://cran.r-project.org/package=emmeans
DESeq2 (v1.26.1)	Love et al. (2014)	https://bioconductor.org/packages/release/bioc/html/DESeq2.html
R (v 3.6.2) R (v 4.0.3)	R Core Team, 2021	https://www.R-project.org/
ggplot2 (v 3.3.3)	Wickham (2016)	https://ggplot2.tidyverse.org/
ROntoTools (v 2.14)	Voichita et al. (2019)	https://bioconductor.org/packages/release/bioc/html/ROntoTools.html
KEGG pathway	Kanehisa (2019); Kanehisa et al. (2021); Kanehisa and Goto (2000)	https://www.genome.jp/kegg/
GraphPad (v9.3.1)	GraphPad, San Diego, USA	https://graphpad.com
Other		
Test placebo	IFPC	Potato maltodextrin

RESOURCE AVAILABILITY

Lead contact

Any further information needed on the resources or reagents used should be directed to the lead contact Charles Budinoff (Charles.R.Budinoff@iff.com).

Materials availability

This study did not generate any unique materials or reagents.

Data and code availability

- Data regarding the entire project is available from Gene Expression Omnibus (GEO) under the SuperSeries number GEO: GSE180391. Individual datasets are also available from GEO for the ferret qPCR (GEO: GSE180390) and human RNA-seq (GEO: GSE180389) studies.
- This paper does not report original code involved in the analysis of the data.
- Any additional information required to reanalyze the data reported in this paper is available from the lead contact upon request.

EXPERIMENTAL MODEL AND SUBJECT DETAILS

Probiotic strains and placebo

The probiotic strains used in the experiments were for OL-1: *Bifidobacterium longum* subsp. *infantis* Bi-26, Danisco Global Culture Collection (DGCC)11473, *Bifidobacterium animalis* subsp. *lactis* Bl-04, American Type Culture Collection (ATCC) Safe Deposit (SD)5219, DGCC2908, *Lacticaseibacillus paracasei* subsp. *paracasei* Lpc-37, SD5275, ATCC PTA-4798, *Lacticaseibacillus rhamnosus* Lr-32, SD5217, and *Ligilactobacillus salivarius* Ls-33, SD5208, and for OL-2: *Bifidobacterium animalis* subsp. *lactis* Bi-07, SD5220, DGCC

2907, *Lactobacillus acidophilus* NCFM, SD5221, ATCC 700396, *Limosilactobacillus fermentum* SBS-1, DGCC1925, *Lactococcus lactis* subsp. *lactis* LI-23, DGCC8656, *Streptococcus thermophilus* subsp. *thermophilus* St-21, SD5207.

For ferret studies, potato maltodextrin was used as a placebo and probiotics were delivered as freeze-dried powder in a capsule that was opened, resuspended to saline, and gavaged. All the strains are owned by and were manufactured along with placebo by IFF (Madison, Wisconsin, USA).

For *in vitro* cell stimulation assay, *Bifidobacterium* strains were cultured anaerobically at 37°C in *Bifidobacterium* medium 58 (Deutsche Sammlung von Mikroorganismen und Zellkulturen, DSMZ) (Salli et al., 2021). Bacteria belonging to *Lacticaseibacillus, Ligilactobacillus, Limosilactobacillus, Lactobacillus, Lactococcus, and Streptococcus* genera were cultured anaerobically at 37°C in de Man, Rogosa and Sharpe medium (LAB M Ltd, Lancashire, United Kingdom), except for *Limosilactobacillus fermentum* SBS-1, which was grown aerobically. Strains were grown to logarithmic growth phase, collected by centrifugation, washed once with PBS and suspended to cell culture medium. The optical density (OD)600 was adjusted to correspond to bacteria: host cell ratio of 10:1. The bacteria in the consortia were applied on cells in equal proportions 2+2+2+2+2.

Ferrets

Outbred male ferrets (Triple F Farms, Sayre, PA) were quarantined at IIT Research Institute (IITRI), Chicago, USA for approximately 6-7 days before initiation of the dosing. Animals were approximately 8-11 months of age and were approximately 1.02.0 kg at the initiation of dosing. Animals were maintained in BSL-2 facility and were transferred to BSL-3 before infection. Ferrets were randomly assigned to the different experimental groups. Each group had 10 animals in pilot and 12 in main study. The study was performed under American Association for Laboratory Animal Science (IACUC) protocol #20-031.

Human PBMC derived macrophages and dendritic cells

Monocytes were purified from freshly collected leukocyte-rich buffy coats obtained from four healthy volunteer blood donors through the Finnish Red Cross Blood Service (permission no 46/2016, renewed annually). Before donation anonymous volunteers signed general informed consent where they gave permission for use of their blood in medical care and in research, sex and other demographic information were not available. The use of human blood was approved by the Ethics Committee of the Hospital District of Helsinki and Uusimaa, Finland (216/13/03/00/2016). Human peripheral blood mononuclear cells were isolated by density gradient centrifugation followed by purification of monocytes with $CD14^+$ magnetic beads. To obtain Mfs purified monocytes were plated on 24 well plates 3×10^5 cells/well (Falcon, Corning, NY, USA) and cultured for 7 days in Macrophage-SFM (Gibco, Life Technologies, Grand Island, NY, USA) with recombinant human GM-CSF (Miltenyi Biotec, Auburn, CA, US) 1000 IU/mL and 1% Antibiotic-Antimycotic (Life Technologies, Grand Island, NY, USA) at 37 °C with 5% CO_2. To differentiate monocytes into immature dendritic cells, monocytes were plated on 12 well plates 5×10^5 cells/well (Falcon, Corning, NY, USA) and cultured for 7 days in RPMI-1640 (Sigma-Aldrich, St. Louis, MO, USA) supplemented with 1% Antibiotic-Antimycotic, 10% fetal bovine serum (FBS) (Life Technologies, Grand Island, NY, USA), IL-4 (400 IU/mL) and GM-CSF (1000 IU/mL).

METHOD DETAILS

Ferret studies

Pilot study

From D-21 through study D21, ferrets in group 1 received a daily oral gavage with the OL-1 consortia (20B CFU/strain), and ferrets in group 3 received a daily oral gavage with the Placebo. Ferrets in group 2 received a daily oral gavage with the OL-2 consortia (20B CFU/strain) from study D1 through study D21. The virus was administered intranasally (i.n.) as droplets on study D0. On study D1, D3, D5, D7, and D9 nasal washes were collected. Five ferrets from each OL-1 and placebo groups were necropsied on D0 and five ferrets from each group were necropsied on D5 and D21 in the pilot study.

Main study

From study D-7 through study D10, ferrets in group 1 received a daily oral gavage with the OL-1 consortia (20B CFU/strain), ferrets in group 2 received a daily oral gavage with the OL-2 consortia (20B

CFU/strain), and ferrets in group 3 received a daily oral gavage with the Placebo. Each probiotic capsule was opened and content diluted in 3 mL sterile PBS for each daily oral gavage. 2019 Novel Coronavirus, isolate USA-WA1/2020 (SARS-CoV-2) was used to challenge the ferrets. The viruses were produced by infecting VE6 cells at IITRI with the SARS-CoV-2 and tissue culture infection dose (TCID50) was calculated. The virus in DMEM was administered i.n. as droplets on study day 8. Ferrets were anesthetized with Ketamine/Xylazine for delivery of the virus. A total of 0.5 mL of virus (target of 10^5 TCID50) was delivered to each study ferret. The 0.5 mL dose was split between each nostril (0.25 mL/nare). To confirm the inoculation titer of the virus, aliquots of the prepared virus solution were collected, the aliquots were stored at $\leq -65°C$, and a viral titer assay (TCID50) was performed. On study days D1, D3, D5, D7, D9, and D10 nasal washes were collected. Ferrets were anesthetized with Ketamine/Xylazine, and 0.5 mL of sterile PBS containing penicillin (100 U/mL), streptomycin (100 μg/mL) and gentamicin (50 μg/mL) were injected into each nostril and collected in a specimen cup when expelled by the ferret. The recovered nasal wash was collected, volume recorded, and aliquoted. One aliquot (~100 μL) was treated with DNA/RNA Shield (Zymo Research, Irvine, CA) and then stored at room temperature for determination of viral load by RT-qPCR. Five ferrets from each group were necropsied on D5, and remaining ferrets from each group were necropsied at D10 in the main study. Lungs were collected and 0.5-1.0 cm^3 piece of lung was flash frozen, and then stored at $\leq -65°C$. The duodenum was harvested, cut longitudinally to expose the inner mucosal layer, rinsed with sterile PBS, and divided into five roughly equal portions. Samples were flash frozen and stored at $\leq -65°C$ for RNA isolation and samples were fixed in 10% formaline for IHC.

RT-qPCR SARS-CoV-2 titers

The concentration of virus in nasal washes from study days D1, D3, D5, D7, D9, and D10 was determined by RT-qPCR assay. Briefly, RNA was extracted from samples stored in RNA/DNA Shield using the Quick-RNA Viral Kit (Zymo Research) according to manufacturer's protocol. RNA was eluted with 100 μL nuclease-free water. A standard curve was prepared by using blank ferret nasal wash collected from ten naive ferrets and spiked with known concentrations of viral RNA. Each RT-qPCR plate included 9 RNA standards (5×10^7, 5×10^6, 5×10^5, 5×10^4, 5×10^3, 5×10^2, 50, 20, 5 copies per RT-qPCR well) in duplicate, a NTC (no template control) and a positive control in triplicate well. Each test sample was analyzed in duplicate wells.

RT-qPCR was performed using the iTaq universal probes onestep kit (Bio-Rad). 5 μL viral RNA was used for RT-qPCR. Total reaction volume was 15 μL (5 μL RNA +10 μL master mix). The following RT-PCR cycling conditions will be used: 50°C for 15 min (RT), then 95°C for 2 min (denature), then 40 cycles of 10 s at 95°C, 45 s at 62°C.

Primers used for SARS-CoV-2 detection:

2019-nCoV_N1-F 5′-GACCCCAAAATCAGCGAAAT-3′

2019-nCoV_N1-R 5′-TCTGGTTACTGCCAGTTGAATCTG-3′

Probe: 2019-nCoV_N1-P: 5′-FAM-ACCCCGCATTACGTTTGGTGGACC-BHQ1-3′

Gene expression analysis by qPCR

Lung and duodenum were collected and stored in trizol. Tissue RNA was isolated using Direct-Zol RNA Miniprep Plus kit. Two step RT qPCR were used to analyze the gene expression in ferret lung and duodenum total RNA samples. Reverse transcription was performed with iScript Reverse Transcription Supermix (Bio-Rad). For lungs, 1250 ng RNA per 50 μL RT reaction and for duodenum, 625 ng RNA per 50 μL RT reaction was used. The total RT reaction volume was 50 μL and RT was performed in a 96 well plate on a Bio-Rad CFX96 Touch Real Time PCR Detection System. After RT, the cDNA was diluted with nuclease free water to bring the final total volume up to 200 μL (4× dilution). 5 μL of diluted cDNA was used for qPCR analysis of the expression of gene of interest. The total PCR reaction volume was 15 μL per well (10 μL master mix + 5 μL cDNA sample) and the qPCR was performed on the CFX384 Touch Real-Time PCR Detection System (Bio-Rad) using the cycling conditions listed below:*60°C for CCL2, IFNα, IFNL1, and IL8.

Temperature	Time	Cycle(s)
95°C	2 min	1
95°C	10 s	40
*60°C or 62°C	45 s	

62°C for all other genes (CCL5, CXCL10, IFNγ, IL10, IL1β, IL6, TLR8, TNFα, ACE2, and RPS18)

Each plate contains a positive control (prepared from stimulated ferret PBMC cells) in duplicate wells, an NTC in duplicate wells and all test samples in duplicate wells. Primer and probe sequences can be found in Table S3.

The threshold baseline of the qPCR assay was manually set at 200 for all plates if the automatically calculated (by the CFX Maestro 1.1 software) threshold baseline was >200. The 200-threshold baseline value was determined at the development/qualification stage of RT-qPCR assays of genes of interest. However, if the automatically calculated threshold baseline was <200, then the threshold baseline was directly used. Cq value in each well was also automatically calculated by the Maestro 1.1 software based on the threshold baseline. Data generated by the software were exported to a Microsoft Excel (Microsoft Corporation; Redmond, WA) spreadsheet for data processing.

dCq was calculated by subtracting cytokine mRNA gene level from that of GAPDH. Then ddCq was obtained by subtracting dCq from placebo group results. The distribution of dCq (grouped by gene, tissue, and day) was then examined for normality (Shapiro test and qq plot) and extremes (< 1Q-3×IQR or > 3Q+3-×IQR). After removal of extremes, mixed effects models were performed for each gene:

$$dCq=ß\_0+ß\_1\times Treatment+ß\_2\times Day+ß\_3\times Animal.ID+Interactions+\varepsilon$$

If the interaction effect Treatment×Day was significant, ANOVA was carried out to compare dCq across three treatment groups within the same tissue and day, followed by post-hoc analysis through obtaining estimated marginal means (EMMs) (Lenth et al., 2021) and pairwise comparison thereof. The multiple comparison p-values were adjusted by Benjamini-Hochberg (BH) method. Log2 fold change was calculated using the log2 of the ratio of EMM dCq test/EMM dCq control. For EMM dCq control we used the placebo for each gene at the same time point or the pre-infection D0 placebo time point for each gene tested.

Immunohistochemical analysis of duodenum for ACE2 expression

Tissue samples were collected from PBS control and SARS CoV-2 -infected ferrets and incubated in 10% neutral-buffered formalin for fixation before they were embedded in paraffin based to standard procedures. The embedded tissues were sectioned and dried for 3 days at room temperature. To detect the ACE2 by immunohistochemistry, Goat Anti-ACE2 antibody (R&D, Cat#: AF933, Lot#: HOK0620051) was used as the primary antibody. Antigen was visualized using citrate buffer (pH6.0), microwaved for 3 min and steam for 15 min.

Slides were viewed and digitized pictures were taken by Olympus VS120 scanner and analyzed by a senior Pathologist using Olyvia 3.2 software (Olympus Corporation, Tokyo, Japan).

Cell stimulation assay

Differentiated Mfs and DCs, from four blood donors (no technical replicates) were stimulated with consortia alone (bacteria: cell ratio of 10:1) or in combination with TLR ligand blend, pIC, 30μg/mL + R848, 10 μM (both from Sigma-Aldrich, St. Louis, MO, USA) for 24 h (Mf) or 48 h (DC). Mfs or DCs without stimulation were used as a control, dimethyl sulfoxide (DMSO), a carrier for the TLR-ligands, were used as a control for pIC+R848 containing treatments.

Enzyme linked immunosorbent assay

Cell culture supernatants from Mf and DC cultures are analyzed for IFN-γ, IL-1β, IL-6, IL-10, IL-12p70, and TNF-α by Quanterix Human Corplex Cytokine 7-Plex Array (Quanterix, Inc., Billerica, MA, USA). In addition,

DC supernatants were analyzed for IL-23 and TGF-β by Quanterix Human 1-plex Assays according to manufacturer's instructions. Results were analyzed with CiraSoft software (Quanterix).

RNA extraction

Monocyte-derived macrophages and DCs were lysed upon collection with MagMAX™ Lysis/Binding Solution (Invitrogen, Thermo Fisher Scientific) and frozen in −80°C. RNA was extracted with KingFisher Flex automated extraction instrument (Thermo Scientific, Thermo Fisher Scientific Inc. Waltham, MA, USA) using MagMAX™-96 Total RNA Isolation Kit (Invitrogen, Thermo Fisher Scientific) following manufacturer's instructions. The RNA quality and quantity were analyzed with Agilent 4200 TapeStation System (Agilent, Santa Clara, CA, USA).

Transcriptomics

Targeted RNA-seq library preparation was conducted with Tempo-Seq (BioSpyder) detector oligonucleotides designed to target all human genes (~23,000). Library preparation was conducted according to BioSpyder kit user manual. 40 Samples were pooled, purified, quantitated and stored frozen prior to sequencing. The pooled libraries were sent to Roy J. Carver Biotechnology Center at the University of Illinois at Urbana-Champaign for TempO-Seq sequencing using the Illumina NovaSeq platform (1 × 50 nt). The target read-depth per sample was 5 million reads with the minimum reads per sample at 1 million. The reads were quality filtered, trimmed and demultiplexed and aligned to the BioSpyder Human Whole Transcriptome v2.0 annotated reference using Salmon (v1.1.0)(Patro et al., 2017). Two samples did not pass the 5 million read minimum, which were both from pIC+R848 treated DC and were not included in the analysis. 38 total samples were processed, sample quality metrics for RNA quality and alignment to the reference can be found in Table S4.

QUANTIFICATION AND STATISTICAL ANALYSIS

Viral titer analysis

The area under the curve (AUC) over the 10 days post infection was calculated from the viral titer trend lines for each ferret using the R statistical programming language. Kruskal-Wallis nonparametric test was performed to evaluate the differences in the AUC among the three treatment groups (sig. level = 0.05), and post-hoc pairwise Wilcoxon tests were deployed for multiple comparisons using Benjamini-Hochberg method for p-value adjustment.

Quantitative PCR

The qPCR dCq values were calculated based on the GAPDH housekeeping gene. Mixed-effect linear models were fit to test for differences between the treatments and control, fitting the model of dCq value = Treatment + Day + (1|Animal ID), with the animal ID being the random effect. The package emmeans (v 1.6.1) (Lenth et al., 2021) was used to conduct post-hoc tests and pairwise comparisons of the treatments, with p-values corrected using the Benjamini-Hochberg method.

Histopathological examination of duodenum

ACE2 expression was scored by using H-score. The H-score is based on a predominant staining intensity. The Intensity scores are classified as negative (0), low intensity (2), medium intensity (2) and high intensity (3). The percentage of cells at each staining intensity level is counted (estimated), and finally, an H-score is assigned using the following formula:

$$\text{Total H Score} = 1 \times (\%\ \text{cells}\ 1+) + 2 \times (\%\ \text{cells}\ 2+) + 3 \times (\%\ \text{cells}\ 3+)$$

Data was presented as mean ± SEM. Statistical analysis was performed using one-way, ANOVA followed by Dunnett's multiple comparisons test. ns, not significant, **, $p < 0.01$; ***, $p < 0.001$. Graphs were generated with GraphPad Prism (GraphPad, San Diego, USA).

Enzyme linked immunosorbent analysis

The data from immune cell ELISA analyses (Figure 4) were log2-transformed prior to statistical analysis. The data were analyzed using a linear model that included the main effects of treatment and donor (2-way ANOVA). Pairwise-comparisons between the treatments were performed using contrasts of estimated marginal means and corrected for false positive rate using Sidak's method. The fit of the models was checked by inspecting the normality of the model residuals. One extreme low value was removed from

the analysis to meet model assumptions (DC: DMSO, IL-23). The analysis was performed using R version 4.0.3 and graphs were generated with GraphPad Prism.

Transcriptomics

Differential expression analysis was conducted using DESeq2 (v1.26.1)(Love et al., 2014) in R (v 3.6.2). Mf and DC data were analyzed separately, as initial PCA determined the cell types to have distinct expression profiles. Donor and treatment were included in the final DESeq2 model of expression = donor + treatment. Genes were considered differentially expressed if the adjusted pvalue < 0.1 and the absolute value of the log2 fold change >1. Principal component analysis (PCA) was performed to determine overall relatedness of the samples under the various experimental conditions using ggplot2 (v 3.3.3) (Wickham, 2016). Pathway analysis was performed using ROntoTools (v 2.14) (Voichita et al., 2019) with a KEGG pathway (Kanehisa, 2019; Kanehisa et al., 2021; Kanehisa and Goto, 2000) considered significantly changed with a false discovery rate perturbation value of >0.1.